University of Warsaw

Faculty of Physics

Michał Marynowski

Record book number: 421451

Simulation of magneto-optical traps for caesium, potassium and silver atoms

Master's thesis in the field of Physics (Studies in English) within MISMaP

The thesis was written under the supervision of

Dr. Mariusz Semczuk

Institute of Experimental Physics

Warsaw, December, 2024

Summary

This thesis focuses on simulating and numerically optimizing the laser cooling and trapping processes for cesium, potassium, and silver atoms. The process begins with the release of atoms from a dispenser source in the case of cesium and potassium, or from a dispenser-like oven for silver. The simulations aim to estimate the performance of magneto-optical trapping in a two-dimensional trap, followed by loading of a three-dimensional magneto-optical trap for each considered atom type. The main objective of these simulations is to verify the initial assumptions that have been made during the design of a new experimental apparatus aiming at the study of ultracold KAg and CsAg molecules. Importantly, the concept of a two-dimensional magneto-optical trap for silver remains unexplored in existing literature, thus simulations are essential to assess its capability in providing precooled silver atoms to load a three-dimensional magneto-optical trap. These simulations enable the analysis of trapping rates, capture velocities, atomic flux, and velocity distributions.

To validate the model, we conducted simulations based on well-known experimental setups developed by other research groups. To illustrate the simulation's adaptability, each scenario involved a unique configuration of experimental parameters for atoms of interest, specifically K, Cs, and Ag. The program produced values that reproduced published results very well.

The simulation models the time-dependent motion of atoms under the influence of laser light and magnetic field. It utilizes a modified version of the AtomECS Rust package, which incorporates the attributes of these fields to compute atomic

trajectories, a Python script for evaluating atomic motion, and a Matlab procedure that executes Bayesian optimization and data visualization. Moreover, the thesis elaborates on the fundamental theory of atom-light interactions, atomic sources, and population statistics within a magneto-optical trap. It discusses various methodologies for assessing the trapping rate in such traps. Lastly, the thesis suggests potential enhancements to the software to improve optimization, make it more user-friendly, and permit the concurrent simulation of traps with differing properties.

Streszczenie

Niniejsza praca skupia się na symulacji i numerycznej optymalizacji procesu chłodzenia laserowego i pułapkowania atomów cezu, potasu oraz srebra. Proces rozpoczyna się od uwolnienia atomów z dyspensera w przypadku cezu i potasu lub z pieca przypominającego dyspenser w przypadku srebra. Symulacje mają na celu oszacowanie wydajności pułapkowania w dwuwymiarowej pułapce magneto-optycznej, a następnie wypełnienia atomami trójwymiarowej pułapki magneto-optycznej dla każdego z rozważanych typów atomów. Głównym celem tych symulacji jest weryfikacja założeń początkowych przyjętych podczas projektowania nowego układu eksperymentalnego, mającego na celu badanie ultrazimnych cząsteczek KAg i CsAg. Co istotne, koncepcja dwuwymiarowej pułapki magneto-optycznej dla srebra nie była jak dotąd rozważana w istniejącej literaturze, dlatego symulacje są kluczowe dla oceny jej zdolności do dostarczania wstępnie schłodzonych atomów srebra do wypełnienia atomami trójwymiarowej pułapki magneto-optycznej. Symulacje te umożliwiają analizę szybkości pułapkowania, prędkości przechwytywania, strumienia atomowego oraz rozkładów prędkości.

W celu walidacji modelu przeprowadzono symulacje oparte na dobrze znanych układach eksperymentalnych opracowanych przez inne grupy badawcze. Aby zilustrować elastyczność symulacji, każdy scenariusz uwzględniał unikalną konfigurację parametrów eksperymentalnych dla badanych atomów, w szczególności K, Cs i Ag. Program wygenerował wartości, które bardzo dobrze odtwarzały wyniki opublikowane w literaturze.

Symulacja modeluje zależny od czasu ruch atomów pod

wpływem światła laserowego i pola magnetycznego. Wykorzystuje zmodyfikowaną wersję pakietu AtomECS napisanego w języku Rust, który uwzględnia właściwości tych pól do obliczania trajektorii atomów, skrypt w Pythonie do obliczania ruchu atomów oraz procedurę w Matlabie do wykonywania optymalizacji bayesowskiej i wizualizacji danych.

Ponadto w pracy omówiono podstawową teorię interakcji atom-światło, źródeł atomowych oraz statystyki populacji w pułapce magneto-optycznej. Przedyskutowano również różne metody oceny szybkości pułapkowania w takich układach. Na koniec praca proponuje potencjalne ulepszenia oprogramowania w celu usprawnienia optymalizacji, zwiększenia przyjazności dla użytkownika oraz umożliwienia równoczesnej symulacji pułapek o różnych właściwościach.

Keywords

2D+ MOT, caesium, potassium, silver, trap, laser cooling, simulations

Title of the thesis in Polish language

Symulacja pułapek magneto-optycznych cezu, potasu i srebra

Contents

Introduction

Atoms constitute the fundamental building blocks of all matter. For centuries, philosophers and physicists alike were fascinated by its underlying structure. Our perception of what we are made of has evolved greatly over time. Already 500 years BCE, Leucippus and Democritus considered the idea of existence of an indivisible core of matter [1]. The term "atom" originates from the Greek word for "indivisible". Although Robert Boyle reintroduced the concept in the 17th century [2], it was not until the 19th century that John Dalton proposed a contemporary atomic model [3]. Up to that point, the atomic structure had not been experimentally examined. The first to do so were J.J. Thomson [4] and Ernest Rutherford [5]. Thomson discovered the electron and Rutherford with his experiments proposed the idea of electrons orbiting a dense nucleus. Until that time, atoms were more or less seen as groups of solid spheres, which still maintained the ideas of the great Greeks. This has changed with the works of Erwin Schrödinger [6] and Werner Heisenberg [7]. They have proposed the wave-particle duality and the probabilistic nature of atomic behaviour. Schrödinger stated his famous equation that describes electron distributions through probability clouds. This wave-particle duality has many consequences, one of which is the Bose-Einstein condensate (BEC). Theoretically, it was proposed by Einstein [8] who used photon statistics developed by Satyendra Bose [9] and applied to atoms. To create a BEC in a laboratory, the atomic cloud had to be dense (of order 10^{13} atoms/cm^3) and greatly cooled ($T < 1$ μK). To do so, experimental physics had to develop groundbreaking techniques starting with Doppler cooling in 1975 by T. W. Hänsch [10]. This allowed a reduction in the velocity of the atoms and the achievement of temperatures in the mK and even μK regime. Further enhancement was a magneto-optical trap (MOT) which allowed us not only to cool but also to trap atoms and increase their density [11]. Those advances led to the creation of the first BEC in 1995 by Eric Cornell and Carl Wieman [12].

With an understanding of quantum mechanics, the need arises to simulate those processes, but there is a significant problem. The quantum state of a system is described by multiple variables which grow exponentially with the number of particles or the degrees of freedom. A solution for this problem was hypothesized by Richard Feynman in 1982 [13] and later developed by Lloyd [14] - a quantum computer. It was to simulate a quantum system with an ensemble of well-defined qubits that could be initialized, and measured, and on which universal quantum gates could be performed. This would act as a universal quantum simulator. A simpler version would be to reproduce the quantum system that we want to understand with a system that we can measure directly [15], a problem-specific quantum simulator. One of the ways to realize it is with polar molecules [16]. The advantage of polar molecules is that their large electric dipole moments produce strong dipole-dipole interactions that can be manipulated relatively easily via external DC and AC microwave fields. Now the task is to create cooled down polar molecules that will have strong dipole moments. It can be done by separately cooling the component atoms and then combining them. In nature atoms, while colliding, can temporarily combine when the energy of the collision is equal to the bound-state energy (such energy corresponds to the Feshbach resonance [17]).

Using an external electromagnetic field, the bound-state energy can be tuned to match collision energy, which will create a weakly bound ultracold molecule. Now the question stands, which molecules have the highest dipole moment?

Motivation

One of the promising platforms for creating a quantum simulator are ultracold ground state molecules with a high electric dipole moment. Very strong candidates are KAg and CsAg which have permanent electric dipole moments on the order of $8.5 - 9.75$ D [18]. When composed of two alkali metals, the electric dipole moments are significantly smaller, reaching 5.5 D for LiCs [19]. However, these molecules have not been produced yet under conditions suitable for modern ultracold experiments.

In order to form KAg or CsAg molecules, we need to characterize the properties of K+Ag and Cs+Ag mixtures and establish a procedure of production of these molecules in their ground states. To achieve that, we must simultaneously laser cool silver and caesium or potassium. This requires an experimental setup, which will provide a trapped cooled gas of each of these elements. We plan to use two 2D magneto-optical traps as sources of pre-cooled atoms that will load a 3D magneto-optical trap. For caesium and potassium, 2D magneto-optical traps for each species have been demonstrated by several groups [20, 21, 22, 23, 24] and are commonly used. The technology is well-established but for a new design, there are many variables that can influence the final outcome of any specific design. For example, solely increasing the size of the cooling beams decreases the intensity but increases the capture range of atoms, and it is not straightforward to answer if the desired outcome, for example an increase in the atom flux, will be achieved. Numerical simulations help to address such concerns. A need for simulations is even more important for laser cooling of silver, because there is no literature reference for the operation of a 2D MOT for this species. The first and only published result for a magneto-optical trap for silver comes from the group of H. Walther [25]. They loaded a magneto-optical trap directly from hot sources (effusion cell and a dispenser). A newer approach for trapping silver that uses a Zeeman slower has been demonstrated recently by David DeMille's group, which also employs a silver MOT [26, 27]. A Zeeman slower requires the ability to send a laser beam counter-propagating with the atomic beam, which requires an optical access (e.g a window) on the opposite of the atomic source. A relatively high flux of atoms from the Zeeman slower can easily coat the window with silver, reducing its transmission and quickly deteriorating the cooling performance. DeMille's group has addressed this by heating the window which complicates the setup and introduces additional variables that make estimating the outcome even more challenging. An alternative solution is to use a 2D trap loaded by a small oven which would provide pre-cooled atoms to load a 3D magneto-optical trap. The high temperature (> 900 °C) required to evaporate silver atoms from a sample poses challenges for this approach. So far, 2D traps with relatively high temperature of the source have been demonstrated for Li [28], Sr [29], and Dy [30], but the temperature for silver will be even higher. This presents a significant technical

challenge, but if successful, it will greatly simplify the experimental setup, reduce energy consumption, and minimise the physical size of the apparatus. With fewer components to fail, a 2D trap is also advantageous for long-term use.

Constructing an experimental setup for laser cooling atoms takes a great deal of time, energy, and equipment. Before this effort, it is worth verifying whether assumptions based on experience have a chance of working. This is why the simulation in the case of silver is even more crucial than in well-researched examples of potassium or caesium sources. Moreover, it will allow us to optimize the system's parameters.

To create the simulation, we have used AtomECS software. It allows us to simulate trajectories of atoms in a single magneto-optical trap. We have modified the software, introducing changes that would allow for the simulation of multiple traps in the same system. Moreover, we have created an analysis script that obtained the velocity distribution of an atomic beam and, with the model of different types of atomic sources, calculates the simulated flux. Additionally, we have performed an optimization of the setup.

Thesis outline

Chapter 1: We start with an explanation of the basic theory that describes the principles of magneto-optical trapping such as dipole force, selection rules, Doppler and Zeeman effects, and optical molasses. We also introduce the theoretical limits of this kind of cooling.
Chapter 2: The theory of atomic sources is provided. It explains how atoms can be introduced into the system and how they will behave in a vacuum. We describe the main types of sources used in atomic cooling, like effusion cells (in the ideal and non-equilibrium cases) and background gas loading.
Chapter 3: We provide mathematical models describing the loss mechanisms for the atomic beam. We discuss what is the reason for the decrease in flux between the effusion cell and the MOT. Additionally, we will show loss mechanisms inside the trap and different approaches for population statistics.
Chapter 4: We present the characteristics of potassium, silver, and caesium that are relevant to the simulation. We explain the basics of simulating magneto-optical traps. We describe different approaches to simulation, and with an exemplary script we show how our program is built.
Chapter 5: We describe the experimental configurations implemented by other research groups to introduce benchmarks for our simulations. The simulation of these experiments is compared with real data extracted from references in the literature, providing a verification that the developed program returns trustworthy results.
Chapter 6: We describe a novel experimental setup constructed in our group which will be used for creating ultracold cold CsAg KAg molecules, and present optimized parameters with the estimated flux, capture velocity, and trapping efficiency that we compare to the results of other setups.

1 Light-matter interaction principles for MOT

Simulating a physical phenomenon must be entirely based on the established laws that describe it. Additionally, it requires us to present our understanding clearly and transparently, highlighting our assumptions. This chapter outlines the theory of how atoms interact with light and how this interaction can be utilised for cooling. It then explains the theory of how magnetic fields influence the atomic energy structure and their application in trapping atoms.

1.1 The steady state solutions for an atom at rest

Let's consider an atom as a quantum object. It is determined by its Hamiltonian H_0, which has eigenstates of eigenfunctions Φ_n and energies $E_n = \hbar\omega_n$ following the connection $E_n\Phi_n = H_0\Phi_n$. Inserting the atom in a laser light adds a time-dependent term $H'(t)$. It leads to the mixing of the stationary eigenstates and so the atom's wavefunction should be written as

$$\Psi(t) = \sum_n c_n(t)\Phi_n \mathrm{e}^{-i\omega_n t}, \tag{1.1}$$

where $|c_n(t)|^2$ is the occupation probability of each state describing the atom's behaviour. To calculate them we substitute 1.1 to the time-dependant Schrödinger's equation

$$H\Psi(t) = i\hbar\frac{\partial}{\partial t}\Psi(t), \tag{1.2}$$

where $H = H_0 + H'(t)$. After differentiating with respect to time and expanding the Hamiltonian, we obtain

$$\begin{aligned} \hbar\omega_n \sum_n c_n(t)\Phi_n \mathrm{e}^{-i\omega_n t} + H'(t)\sum_n c_n(t)\Phi_n \mathrm{e}^{-i\omega_n t} = \\ i\hbar\sum_n \dot{c}_n(t)\Phi_n \mathrm{e}^{-i\omega_n t} + \hbar\omega_n \sum_n c_n(t)\Phi_n \mathrm{e}^{-i\omega_n t}, \end{aligned} \tag{1.3}$$

where we also used the connection between the energy and H_0. The two terms with $\hbar\omega_n$ cancel each other out. The next step is to multiply by Φ_j and sum over all eigenstates. For the sum of $\dot{c}_n(t)$ the only non-zero term is for $n = j$, since the eigenstates are orthogonal. The interaction Hamiltonian $H'(t)$ becomes $H'_{jn} \equiv \langle\Phi_j| H'(t) |\Phi_n\rangle$. The final equation for transformed time-dependant Schrödinger's equation is

$$\dot{c}_j(t) = \frac{1}{i\hbar}\sum_n c_n(t)H'_{jn}(t)\mathrm{e}^{i\omega_{jn}t}, \tag{1.4}$$

where $\omega_{jn} \equiv \omega_j - \omega_n$. In the above equation, the remaining unknown is the interaction Hamiltonian. To calculate it further we need to describe the system more accurately. Our atom is a two-level system and we take on a semi-classical approach that quantises the atom's structure and assumes light's wave nature. We start with describing a Hamiltonian of an atom:

$$H(t) = \frac{1}{2m}(\vec{p} + e\vec{\mathcal{A}})^2 + V, \tag{1.5}$$

where $\vec{p}$ is the momentum of the electron in the atom, m is its mass, e is its charge, and $\vec{\mathcal{A}}$ is the vector potential of the magnetic field.

We choose the Coulomb gauge where the $\vec{\nabla}\vec{\mathcal{A}} = 0$. From the definition of momentum $\vec{\nabla} = 1/i\hbar \cdot \vec{p}$, and so $\vec{\mathcal{A}}$ and $\vec{p}$ commute. We obtain

$$H(t) = \frac{1}{2m}(\vec{p}^2 + 2\vec{\mathcal{A}} \cdot \vec{p} + \vec{\mathcal{A}}^2) + V. \tag{1.6}$$

We can now compare the amplitudes of the field and the atom momenta by taking their ratio. We substitute $|\vec{\mathcal{A}}| = 1/\omega \cdot |\vec{\mathcal{E}}|$, which comes from the relation $\vec{\mathcal{E}} = -\frac{\partial \vec{\mathcal{A}}}{\partial t}$. For the comparison, we take a ground state hydrogen whose electron's momentum is $|\vec{p}| = \hbar/a_0$. This leads to

$$\frac{|e\vec{\mathcal{A}}|}{|\vec{p}|} = \frac{e|\vec{\mathcal{E}}a_0|}{\hbar\omega} \approx 7 \cdot 10^{-8}, \tag{1.7}$$

where a_0 is the Bohr's radius. In order to approximate the amplitude of the electric field we took the parameters of a typical laser beam used for trapping atoms, with $\lambda = 500$ nm, beam radius of 10 mm, and power of 100 mW. This comparison shows that $|e\vec{\mathcal{A}}|$ is much smaller than the electron's momentum so we can set the term $\vec{\mathcal{A}}^2$ as 0 leaving only

$$H(t) = \frac{\vec{p}^2}{2m} + V + \frac{e\vec{\mathcal{A}} \cdot \vec{p}}{m} = H_0 + H'(t). \tag{1.8}$$

This sets the interaction Hamiltonian to be $H'(t) = e\vec{\mathcal{A}} \cdot \vec{p}/m$. The vector potential can be written as

$$\vec{\mathcal{A}}(t) = \frac{1}{2}\mathcal{A}_0 \exp\Big[i(\vec{k} \cdot \vec{r} - \omega t + \phi)\Big] + c.c, \tag{1.9}$$

where ϕ is an arbitrary phase. We want now to simplify it by making the vector potential position independent using the rotating wave approximation. For that let's expand the exponent according to Taylor's series: $\exp(ik \cdot r) = 1 + i\vec{k} \cdot \vec{r} + O\left(\vec{k} \cdot \vec{r}\right)^2$ and consider how the potential changes throughout the range of the electron's movement. Argument r would have the order of an Angstrom - 10^{-10}

and so the product $|\vec{k}\cdot\vec{r}| = \frac{2a_0}{\lambda} \approx 0.0005$ for visible light at $\lambda = 500$ nm. This allows us to treat the expanded exponent as unity. It is called electric dipole approximation (EDA). It makes the vector potential constant for the area of an atom giving

$$\vec{\mathcal{A}} = \mathcal{A}_0 \cos(\omega t + \phi)\hat{\varepsilon}. \tag{1.10}$$

We can calculate the interaction Hamiltonian between the ground and the excited state as

$$H'_{eg}(t) = \langle e| H'(t) |g\rangle = \frac{e}{m} \langle e| \vec{\mathcal{A}}(t)\cdot\vec{p}|g\rangle \approx \mathcal{A}_0 \cos(\omega t + \phi)\hat{\varepsilon}\cdot\langle e|\vec{p}|g\rangle . \tag{1.11}$$

Momentum can be determined using the Heisenberg equation of motion giving:

$$H'_{eg}(t) = \mathcal{A}_0 \cos(\omega t + \phi)\hat{\varepsilon}\cdot\langle e|\frac{im}{\hbar}[H_0,\vec{r}]\,|g\rangle . \tag{1.12}$$

We perform simple calculations from the definition of the commutator and obtain eigenvalues of the state

$$\begin{aligned}\frac{ie}{\hbar}\langle e|\,[H_0,\vec{r}]\,|g\rangle = \frac{ie}{\hbar}\langle e|\,(H_0\cdot\vec{r}-\vec{r}\cdot H_0)\,|g\rangle &= \frac{ie}{\hbar}(E_e\langle e|\,\vec{r}\,|g\rangle - E_g\langle e|\,\vec{r}\,|g\rangle)\\ &= -i(\omega_e-\omega_g)\cdot\langle e| - e\vec{r}|g\rangle .\end{aligned} \tag{1.13}$$

The last term in this equation is the matrix element of the dipole operator $\vec{\mu} = -e\vec{r}$. Applying it in the formula and inserting 1.13 to 1.12 gives us

$$H'_{eg}(t) = -i\omega_{eg}\mathcal{A}_0\cos(\omega t+\phi)\hat{\varepsilon}\cdot\vec{\mu}_{eg}, \tag{1.14}$$

where we determine $\phi = -\pi/2$ so that $i\omega_{eg}\mathcal{A}_0\cos(\omega t-\pi/2) = -\frac{\partial\vec{A}}{\partial t}$ which is the electric field $\vec{\mathcal{E}}(t) = \mathcal{E}_0\cos(\omega t)$ based on Maxwell equations. Lastly, we introduce Rabi frequency defined as $\Omega_{eg} \equiv \mathcal{E}_0\hat{\varepsilon}\cdot\vec{\mu}_{eg}/\hbar$, which gives us the final expression as

$$H'_{eg}(t) = \hbar\Omega_{eg}\cos(\omega t). \tag{1.15}$$

We introduce it to 1.4 obtaining

$$\begin{aligned}i\hbar\frac{dc_g(t)}{dt} &= c_e(t)\frac{\hbar}{2}\Omega_{eg}(\mathrm{e}^{i\omega t}+\mathrm{e}^{-i\omega t})\mathrm{e}^{-i\omega_{eg}t}\\ i\hbar\frac{dc_e(t)}{dt} &= c_g(t)\frac{\hbar}{2}\Omega_{ge}(\mathrm{e}^{i\omega t}+\mathrm{e}^{-i\omega t})\mathrm{e}^{i\omega_{eg}t}.\end{aligned} \tag{1.16}$$

Both expressions have only one term since $H'_{gg}(t) = H'_{ee}(t) = 0$. In the above equations, terms like $\exp(-i(\omega + \omega_{eg})t)$, with the sum of the frequencies, we can treat as 0 since they oscillate quickly and average out. This is called the rotating wave approximation (RWA). The remaining terms we can describe with detuning $\delta \equiv \omega - \omega_{eg}$, which represents how far the light's energy is from the transition's. To ease calculations, we perform the rotating frame transformation where $\tilde{c}_e(t) \equiv c_e(t)\mathrm{e}^{i\delta t}$ replaces $c_e(t)$. This gives

$$\begin{aligned} \frac{dc_g(t)}{dt} &= -i\frac{\Omega^*}{2}\tilde{c}_e(t) \\ \frac{d\tilde{c}_e(t)}{dt} &= -i\frac{\Omega}{2}c_g(t) + i\delta\tilde{c}_e(t). \end{aligned} \tag{1.17}$$

1.1.1 The density matrix approach

After calculating the differential equations for coefficients $c_n(t)$ we will use the density matrix formalism to extract measurable information about the system, for example, the force acting on the atom. The density matrix is represented by $\rho = |\Psi\rangle\langle\Psi|$, where each element is $\rho_{ij} = c_i c_j^*$. The diagonal terms describe the probability for an atom to be in a specific state and off-diagonal parts are coherences, which depend on the phase between two states. The expectation value of an operator A using the density matrix can be defined as:

$$\langle A \rangle = \mathrm{Tr}(\rho A). \tag{1.18}$$

The next step is to calculate differential equations for elements of the density matrix using 1.17. Before it we have to include one additional term. The semi-classical approach does not predict spontaneous emission so it has to be added according to the Wigner-Weisskopf model, where the new term is

$$\frac{dc_{e_{spt}}(t)}{dt} = -\frac{\gamma}{2}c_{e_{spt}}(t), \tag{1.19}$$

where $\gamma = \omega^3 e^2 a_0^2 / 3\pi\varepsilon_0\hbar c^3$. It represents a loss in the excited state due to the spontaneous emission. Since the ground state is vastly populated compared with the change due to the spontaneous emission we can think of it as constant so $\frac{dc_{g_{spt}}(t)}{dt} = 0$. From the definition of ρ_{ij}, and equations 1.17 and 1.19 we can derive the optical Bloch equations (OBE) for the resting atom

$$\begin{aligned}
\frac{d\rho_{gg}}{dt} &= \gamma\rho_{ee} + \frac{i}{2}\left(\Omega\tilde{\rho}_{ge} - \Omega^*\tilde{\rho}_{eg}\right) \\
\frac{d\rho_{ee}}{dt} &= -\gamma\rho_{ee} + \frac{i}{2}\left(\Omega^*\tilde{\rho}_{eg} - \Omega\tilde{\rho}_{ge}\right) \\
\frac{d\tilde{\rho}_{ge}}{dt} &= -\left(\frac{\gamma}{2} + i\delta\right)\tilde{\rho}_{ge} + \frac{i}{2}\Omega^*\left(\rho_{gg} - \rho_{ee}\right) \\
\frac{d\tilde{\rho}_{eg}}{dt} &= -\left(\frac{\gamma}{2} - i\delta\right)\tilde{\rho}_{eg} + \frac{i}{2}\Omega\left(\rho_{ee} - \rho_{gg}\right).
\end{aligned} \tag{1.20}$$

When we equal them to 0 and solve them we will achieve the steady-state solutions. Using connections like: the conservation of the population $\rho_{ee}+\rho_{gg} = 1$, the optical coherence $\rho_{eg} = \rho_{ge}^*$, and introducing a new variable, $w \equiv \rho_{ee} - \rho_{gg}$, the population difference, we obtain the solution

$$\rho_{eg} = \frac{-i\Omega}{2(\frac{\gamma}{2} - i\delta)(1+s)} \tag{1.21}$$

$$w = \frac{-1}{1+s}, \tag{1.22}$$

from which one can extract all the other terms of the density matrix. Variable s is the saturation parameter defined as

$$s \equiv \frac{|\Omega|^2}{2|\frac{\gamma}{2} - i\delta|^2}. \tag{1.23}$$

In semi-classical formalism, force is treated as an operator $\langle\mathcal{F}\rangle = \frac{d}{dt}\langle\vec{p}\rangle$. The expectation value for a time-independent operator is described by the Ehrenfest theorem

$$\frac{d}{dt}\langle\vec{p}\rangle = \frac{i}{\hbar}\langle[H;\vec{p}]\rangle = -\left\langle\frac{\partial H}{\partial z}\right\rangle. \tag{1.24}$$

The only direct spatial term lies in the interaction Hamiltonian. We derive its matrix form using 1.17

$$H' = \hbar\begin{bmatrix} i\delta & -i\frac{\Omega}{2} \\ -i\frac{\Omega^*}{2} & 0 \end{bmatrix}. \tag{1.25}$$

When we insert it into 1.21 and use the definition of the expectation value in the density matrix formalism we obtain

$$\langle\mathcal{F}\rangle = -\frac{\partial}{\partial z}Tr\left(\rho H'\right) = -\frac{\partial}{\partial z}\left(-2\delta\rho_{ee} + \rho_{eg}\Omega^* + \Omega\rho_{ge}\right) = -\frac{\hbar}{2}\left(\frac{\partial\Omega^*}{\partial z}\rho_{eg} + \frac{\partial\Omega}{\partial z}\rho_{ge}\right). \tag{1.26}$$

It is a general equation for force for any set of steady-state OBE. Additionally, the derivative can be split into the real and imaginary parts as $\frac{\partial\Omega}{\partial z} = (q_r + iq_i)\Omega$. The derivative can be written as a multiplication with a constant since the full dependence on z is enveloped in an exponent. The final equation for the force is

$$F = \hbar q_r(\Omega\rho_{eg}^* + \Omega^*\rho_{eg}) + \hbar q_i(\Omega\rho_{eg}^* + \Omega^*\rho_{eg}). \tag{1.27}$$

1.2 Moving atom in a standing wave

To pursue calculations we need to dive deeper into our system, which is a neutral atom moving in a standing wave. A standing wave is seen as two plane waves of the same amplitude and opposite directions interfering with each other. Setting the electric field as $\mathcal{E}(z,t) = \mathcal{E}_0 \exp(i(kz - \omega t))$ we can describe the standing wave as

$$\mathcal{E}_{\text{st}}(z,t) = \mathcal{E}_0\left(\mathrm{e}^{i(kz-\omega t)} + \mathrm{e}^{i(-kz-\omega t)}\right) = 2\mathcal{E}_0\cos(kz)\mathrm{e}^{-i\omega t}, \tag{1.28}$$

where we used the exponent representation of a cosine. We can understand that term $\mathcal{E}_0(z) = 2\mathcal{E}_0\cos(kz)$ is a position dependent amplitude. Since the term expressing coupling between the electric field and the atom depends on the amplitude of the electric field it will be $\Omega(z) = 2/\hbar \cdot \mathcal{E}_0\cos(kz)\hat{\varepsilon_0}\vec{\mu}_{eg}$. Then the terms of the derivative will be $q_i = 0$ and $q_r = -k\tan(kz)$. Substituting them to 1.27 provides

$$F = -k\hbar\tan(kz)q_r(\Omega\rho_{eg}^* + \Omega^*\rho_{eg}). \tag{1.29}$$

After introducing the idea of a standing wave into the calculation we need to introduce the notion of atom's movement. For that, we add a small velocity-dependent perturbation, which will provide corrections to the already shown solutions. The Rabi frequency and ρ_{eg} will be

$$\begin{aligned} \frac{d\Omega}{dt} = v\frac{\partial\Omega}{\partial z} = \frac{\partial\Omega}{\partial t} - vk\tan(kz)\Omega \\ \frac{d\rho_{eg}}{dt} = \frac{\partial\rho_{eg}}{\partial t} + v\frac{\partial\rho_{eg}}{\partial z} = \frac{ikv\Omega}{2(\frac{\gamma}{2} - i\delta)(1+s)}\left[\tan(kz)\left(\frac{1-s}{1+s}\right)\right]. \end{aligned} \tag{1.30}$$

The derivative over time equals 0 since it's a perturbation of a steady-state solution whose results are not explicitly time-dependent. After solving the derivative equations and substituting them into 1.29 we obtain an updated velocity equation for the force exerted on the atom

$$F = \hbar k\frac{s_0\delta\gamma^2}{2(\delta^2 + \frac{\gamma^2}{4})}\left[\sin(2kz) + kv\frac{\gamma}{\delta^2 + \frac{\gamma^2}{4}}(1 - \cos(2kz))\right], \tag{1.31}$$

where s_0 is the saturation parameter for both beams in the standing wave. It's equal to the s when detuning is 0. In the force, two periodical terms average out in space. The velocity-dependant term becomes

$$F_{av} = -\beta\vec{v} = \hbar k^2 v \frac{8s_0\delta}{\gamma(1 + s_0 + (\frac{2\delta}{\gamma})^2)^2}. \tag{1.32}$$

Saturation parameter s_0 in the denominator could be left out [31] since it is a case of low intensities ($I \ll I_{sat}$). We have decided to show this version so that it will be compatible with results obtained through other approaches. The presented force in the case of negative detuning $\delta < 0$ is equivalent to a damping force responsible for cooling down atoms.

1.3 Selection rules

The dipole operator is the last term that has to be evaluated to see how the force on the atom depends on the field. It describes the coupling between two states in the electric dipole approximation. It depends on the wave function of the two states in the transition. Approximation to a two-level system does not facilitate the calculation since the states have to be studied closer and we need to calculate it explicitly. Still, the dipole operator yields zero for some specific parameters of the electric field and the states. Set of such combinations is called the selection rules. In order to explore them we need to express the functions explicitly using the well-known solutions for the hydrogen atom represented by the spherical harmonics $Y_{lm}(\theta, \phi)$ and Laguerre polynomials inside the radial part of the solution $R_{nl}(r)$

$$\begin{aligned} |g\rangle &= R_{nl}(r)Y_{lm}(\theta, \phi) \\ |e\rangle &= R_{n'l'}(r)Y_{l'm'}(\theta, \phi). \end{aligned} \tag{1.33}$$

Variables n, l and m are quantum numbers, where n is the principal quantum number describing the overall energy of the electron, and l is the orbital quantum number determining the orbital momentum. Its orientation is represented by the magnetic quantum number m. We pick the basis vectors of the polarisation vector $\hat{\varepsilon}$ as

$$\hat{\varepsilon}_{-1} = \frac{\hat{x} - i\hat{y}}{\sqrt{2}} \qquad \hat{\varepsilon}_0 = \hat{z} \qquad \hat{\varepsilon}_{+1} = -\frac{\hat{x} + i\hat{y}}{\sqrt{2}}. \tag{1.34}$$

They are normalised and mutually orthogonal and we understand them as left-handed circular polarisation σ_{-1}, right-handed σ_{+1}, and a linear polarisation π. Since the wavefunctions are described in the spherical coordinates, where

$$
\begin{aligned}
x &= \rho\cos\phi\sin\theta \\
y &= \rho\sin\phi\sin\theta \\
z &= \rho\cos\phi,
\end{aligned}
\tag{1.35}
$$

we should do the same for $\hat{\varepsilon}$. After substituting 1.35 into 1.34 we see that they can be equally expressed as $\hat{\varepsilon}_q = \sqrt{\frac{4\pi}{3}}Y_{1q}(\theta,\phi)$, where $q = -1, 0, +1$. Ultimately the matrix elements of the dipole operator become

$$
\vec{\mu}_{eg} = \langle e|\,\hat{\varepsilon}_q \cdot \vec{\mu}\,|g\rangle = -e\,\langle e|\,\hat{\varepsilon}_q \cdot \vec{r}|g\rangle =
$$
$$
-e\,\langle R_{n'l'}(r)|\,|r|\,|R_{nl}(r)\rangle\,\langle Y_{l'm'}|\,\sqrt{\frac{4\pi}{3}}Y_{1q}(\theta,\phi)\,|Y_{lm}\rangle\,.
$$

Let's focus only on the angular term that we will call $\mathcal{A}^q_{l'm',lm}$. To see if any combinations of q, l, m will cancel the term we can introduce Wigner 3-j symbolism [32]:

$$
\mathcal{A}^q_{l'm',lm} = (-1)^(l' - m')\sqrt{\max(l,l')}\begin{pmatrix} l' & 1 & l \\ -m' & q & m \end{pmatrix}. \tag{1.36}
$$

Due to the symmetry of the 3j-symbols, this form can be different from zero only when the sum of the bottom terms equals zero. This can be interpreted as the total projection of angular momentum $(m' + q + m)$ must remain invariant under rotations which is the angular momentum conservation law. This is one of the selection rules. It states $\Delta m = 0, \pm 1$. As a result, the right-handed circularly polarised light ρ_+ will excite an electron to a state which differs in the magnetic quantum number by $+1$ and the opposite will happen for the left-handed circularly polarised light ρ_-.

1.4 Influence of the magnetic field on the atom

The provided selection rule suggests that circularly polarised light can selectively excite transitions depending on their magnetic quantum number. Let's now investigate how such states can be created and what is their frequency. We will explain the Zeeman effect. To describe the Hamiltonian of the system we have to start from the beginning going back to the equation 1.6. The vector potential of the magnetic field will be given by $\vec{\mathcal{A}} = \frac{1}{2}(\vec{\mathcal{B}} \times \vec{r})$. Substituting it gives us

$$
H_{ZO} = \frac{e}{2m}\vec{\mathcal{B}} \cdot (\vec{r} \times \vec{p}) + \frac{e^2}{8m}|(\mathcal{B} \times \vec{r})|^2. \tag{1.37}
$$

We can substitute into the equation orbital angular momentum $\vec{l} \equiv \vec{r} \times \vec{p}$, Bohr magneton $\mu_B \equiv e\hbar/2m$ and discard the quadratic element since the shifts of

energies due to the considered external magnetic field are much smaller than the unshifted energies. This provides a form

$$H_{ZO} = \frac{1}{\hbar} g_l \mu_B \vec{l} \cdot \vec{\mathcal{B}}. \tag{1.38}$$

We add the Landé g-factor, an experimentally established constant which for the orbital case is approximately 1. This is the change due to the orbital magnetic moment. It comes from the current associated with electron's movement around the nucleus.

Moreover, the electron has an intrinsic magnetic moment

$$\vec{\mu}_e = -\frac{1}{\hbar} g_e \mu_B \vec{s}, \tag{1.39}$$

where $g_e \approx 2$ and $\vec{s}$ is the spin of an electron. Spin represents the angular moment of the electron. Both spin and the angular moment do not convey literal physical meaning since the electron is a point particle and does not rotate around an axis. They are terms used to describe its magnetic moment. This interaction between the external magnetic field and the intrinsic magnetic moment provides additional changes to the Hamiltonian. They can be calculated similarly to the orbital magnetic momentum

$$H_{ZS} = \frac{1}{\hbar} g_e \mu_B \vec{s} \cdot \vec{\mathcal{B}}. \tag{1.40}$$

.

The final factor influencing the energy structure of an atom is the spin-orbit interaction. It arises from the fact that an electron with a magnetic moment moves in the electric field of the nucleus from which a magnetic field is created $\vec{\mathcal{B}_n} = -1/c^2 \cdot (\vec{v} \times \vec{\mathcal{E}_n})$. This field interacts with the intrinsic magnetic moment giving a shift of $H_{SO} = -\vec{\mu_e} \cdot \vec{\mathcal{B}_n}$. This term will be neglected in our calculations. We are considering a regime where the external field is much stronger than the $\vec{\mathcal{B}_n}$. The final Hamiltonian will be

$$H = H_0 + \frac{\mu_B}{\hbar} (\vec{l} \cdot \vec{\mathcal{B}} + 2\vec{s} \cdot \vec{\mathcal{B}}). \tag{1.41}$$

The frequency shift between each state resulting from the Zeeman effect will be $\omega_Z = \frac{\mu_B}{\hbar} \mathcal{B}$.

1.5 Magneto-optical trap

A one-dimensional magneto-optical trap (MOT) is a standing wave created by two counter-propagating laser beams with opposite circular polarisation, detuned by δ, with an external magnetic field that is linearly dependent. In a MOT we

have a damping force that slows down atoms independent of their initial velocity as stated by 1.42. It is responsible for cooling.

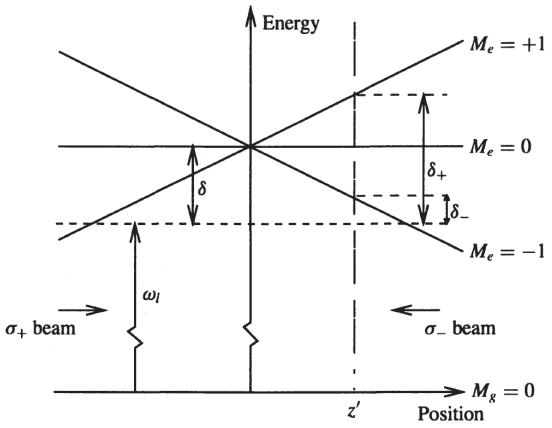

Figure 1: Scheme of energy levels as a function of position for a 1D magneto-optical trap. The detuning δ, δ_-, and δ_+ denote the energy differences between the laser and the respective atomic levels $M_e = -1$, $M_e = 0$, and $M_e = 1$. The position z' represents an example location of an atom. The variable ω_l is the laser frequency, corresponding to the energy of its photons. Adopted from [31].

Based on Fig. 1 we can see what happens to the atom when it is in the trap. In the whole area of the trap, the atom is slowed down by the damping force. At position z' beam ρ_- couples ground state only with $M_e = -1$ due to the discussed selection rule and beam ρ_+ couples $M_g = 0$ only with $M_e = +1$. Since for the position z' magnetic field is positive the state $M_e = -1$ is closer to the excitation wavelength, represented by δ_-, than the state $M_e = +1$. This makes it more probable that the atom will be affected by the photon from the beam ρ_- which will push the atom in the direction of the centre of the magnetic field. This results in trapping. To derive this trapping force we can approximate the frequency shift by $\omega_Z \approx \frac{\mu_B}{\hbar}\nabla\vec{\mathcal{B}} \cdot \vec{r}$ because the magnetic field is 0 for $\vec{r} = 0$. This shift can be introduced into the equation of force by a change in the detuning $\delta \to \delta - \frac{\mu_B}{\hbar}|\nabla\vec{\mathcal{B}} \cdot \vec{r}|$. We have set the sign to a minus since for every position the effective Zeeman shift will be negative. Velocity-dependant force can also be regarded as the result of a detuning shift due to the relativistic Doppler effect. In the variable β we substitute the part of the Doppler shift $|\vec{k} \cdot \vec{r}|$ with the Zeeman shift $\frac{\mu_B}{\hbar}|\nabla\vec{\mathcal{B}} \cdot \vec{r}|$ resulting in a position-dependent trapping force. Two of them added together give the final force experienced by an atom in the magneto-optical trap

$$F = -\beta\vec{v} - \frac{\beta}{k}\frac{\mu_B}{\hbar}|\nabla\vec{\mathcal{B}} \cdot \vec{r}|. \tag{1.42}$$

It is the form of a damped harmonic oscillator, where the damping coefficient is β and the spring constant is $\kappa = \mu_B/\hbar k \cdot \beta\nabla\mathcal{B}$. Presented 1D MOT can be easily extended to a 3D case with 3 pairs of circularly polarised beams.

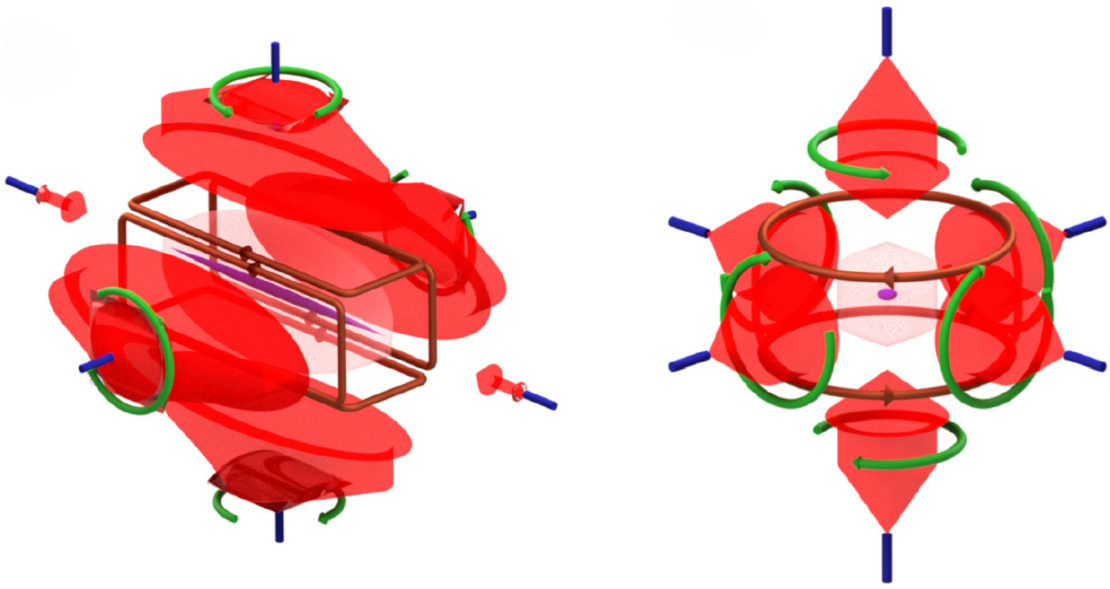

(a) Two dimensional MOT. (b) Three dimensional MOT.

Figure 2: Visualisation of different MOT schemes. Adopted from [33].

1.6 The rate equation model

We presented the forces acting on the atom. We would like to provide a simplified model that allows easy calculation of the force. We treat the atom, as before, as a classical, two-level system with the energy difference between two states being $\hbar\omega_0$. It interacts with the laser by absorbing the photon from an incident laser beam. When it absorbs gains a momentum kick $\hbar\vec{k}$. This occurs at the photon scattering rate [34]

$$R = \frac{I(\vec{r})}{I_{\text{sat}}} \frac{\Gamma}{2} \frac{\frac{1}{4}\Gamma^2}{\delta(\vec{r},\vec{v})^2 + \frac{1}{4}\Gamma^2}, \tag{1.43}$$

where Γ is the natural linewidth, and the Zeeman and Doppler effects are represented by the position and velocity dependence of the detuning. It can be used to calculate density matrix elements, where the population densities of both states are

$$\dot{\rho_{ee}} = -\rho_{ee}A_{21} - \left(\sum_i R_i\right)(\rho_{ee} - \rho_{gg}) \tag{1.44}$$

$$\dot{\rho_{gg}} = \rho_{ee}A_{21} + \left(\sum_i R_i\right)(\rho_{ee} - \rho_{gg}), \tag{1.45}$$

where A_{21} is the Einstein coefficient for decay from the upper level and, for a two-level system, is equal to the natural linewidth Γ, and $\sum_i$ is a sum over each laser. They give steady-state solutions when $t \to \infty$

$$\rho_{ee} = \frac{\sum_i R_i}{\Gamma + 2\sum_i R_i} \tag{1.46}$$

$$\rho_{gg} = 1 - \rho_{ee}. \tag{1.47}$$

The average number of photons scattered in time step Δt by each laser is equal

$$N_i = \frac{R_i}{\sum_i R_i} \Delta t \rho_{ee} \Gamma. \tag{1.48}$$

Then the force from the absorption of the atom becomes

$$F_{A,i} = \frac{\hbar \vec{k_i} n_i}{\Delta t}, \tag{1.49}$$

where n_i is the number of photons scattered based on the Poissonian distribution of an average value N_i. Additionally, the spontaneous emission causes a random walk in the momentum space so a force arises

$$F_{E,i} = \sum_j^{n_i} \frac{\hbar |\vec{k_i}|}{\Delta t} \vec{e}_j, \tag{1.50}$$

where $\vec{e}_j$ is a random unit vector of the emitted photon.

1.7 Limit of laser cooling

A laser beam interacts with an atom when a photon is absorbed by it. Then the atom gains the photon's momentum through fully inelastic collision and after the state's lifetime, the atom emits the photon back in a random direction. Since it is a random spontaneous emission, on average, it doesn't transfer any momentum but results in a random shift of velocity. Analogically, it is in the case of Brownian motion but it happens for the position of a particle not for its momentum. This shift is responsible for a non-zero mean square velocity.

We can calculate this steady-state temperature by assuming that the atom is a particle moving in a viscous media where the momentum step is $\Delta p = \hbar k$ and its rate is $\Delta t = 2\gamma_p$, two times the scattering rate of a single beam

$$\gamma_p = \frac{s_0 \gamma}{2(1 + s_0 + (\frac{2\delta}{\gamma})^2)} \tag{1.51}$$

.

The diffusion coefficient will be [35]

$$D_0 \equiv \frac{2(\Delta p)^2}{\Delta t} = 4\gamma_p(\hbar k)^2 \tag{1.52}$$

.

We can set the damping coefficient as β and using Einstein's equation for Brownian motion calculate the Doppler temperature limit for cooling in an optical molasses

$$T_{\text{lim}} = \frac{D_0}{k_B\beta} = \frac{4\gamma_p(\hbar k)^2}{k_B\beta}, \tag{1.53}$$

which for Caesium 133 atoms would be around 125nK [36].

2 Physics of an atomic source

In considering a magneto-optical trap it is vital to understand different sources of atoms that will replenish the atomic cloud. This chapter will provide an introduction to different types of sources and also the theory that will allow us to simulate the atomic beam on their output. We will only focus on the direct emitters excluding Zeeman slower [37]. As a disclaimer, we would like to note the differences between intensity and flux as flux in atomic physics is defined differently than in, for example, fluid dynamics. Flux Φ is understood as the number of atoms crossing a plane in a unit of time [atoms/s] and the intensity I of the beam is number of atoms crossing area per unit of surface and time [atoms $\cdot$ s^{-1} $\cdot$ m^{-2}].

2.1 Vapour pressure

The most basic source of atoms is background gas. When a material is set in a vacuum in a closed box at temperature T, with time the atoms will evaporate from the material to fill space and set an equilibrium throughout the whole box. The pressure of the gas inside is the vapour pressure [38]

$$p_v = p_0 \exp\left(-\frac{\frac{1}{k_B}H_{\text{vap}}}{T}\right), \tag{2.1}$$

where p_0 is an empirical constant specific to an element, and $\frac{1}{k_B}H_{\text{vap}}$ is the latent heat of vaporisation. The relation can be also represented by a polynomial equation [39]

$$\log(p) = A + B \cdot T^{-1} + C \log T + D \cdot T \cdot 10^{-3}, \tag{2.2}$$

where letters from A to D are fitted constants.

2.2 The ideal effusion cell

The effusion cell (Knudsen cell) is a liquid or vapour closed in a container with a single hole, where the surface area of the liquid is much bigger than that of the orifice. A beam exiting the output is a stream of collision-less atoms called a molecular beam. The name refers to the molecular flow regime of atoms. To call a source an ideal effusion cell it has to fulfil the following assumptions [40]:

1. material in the cell is in thermodynamic equilibrium;
2. the average path where the particle travels undisturbed (the mean free path) is much bigger than the size of the pupil;
3. walls are much thinner than the pupil diameter;
4. pupil diameter is smaller than the distance to the receiving spot;
5. the pupil is flat.

Thermodynamic equilibrium means that atoms have a Maxwell-Boltzmann velocity distribution and that the vapour pressure of thermodynamic equilibrium is present throughout the cell. The assumption about the mean free path ensures that atoms leave the cell without colliding with each other. Assumption 3 does the same for collisions with the walls of the pupil. Assumption 4 ensures that particles arrive as if from a single-point source for the receiving surface. Using those notions we can assume that there is thermodynamic equilibrium between the vapour and outer regions of the cell. In such a case, the number of collisions of atoms with the walls of the cell can be used as a measure of the intensity of the beam emitted from the cell. The kinetic theory describes it as impingement rate [38]

$$I = \frac{p}{\sqrt{2\pi m k_B T}}, \tag{2.3}$$

where p is the pressure of the gas, m is the mass of the atoms, and T is the temperature. The distribution of the flux depending on the polar angle θ and azimuthal angle ϕ is described by Knudsen's cosine law for the beam's intensity

$$\Phi_\Omega(\theta, \phi) = Ia\frac{\cos\theta}{\pi}, \tag{2.4}$$

where a is the small area of the pupil. Martin Knudsen proposed and proved it in 1915 [40].

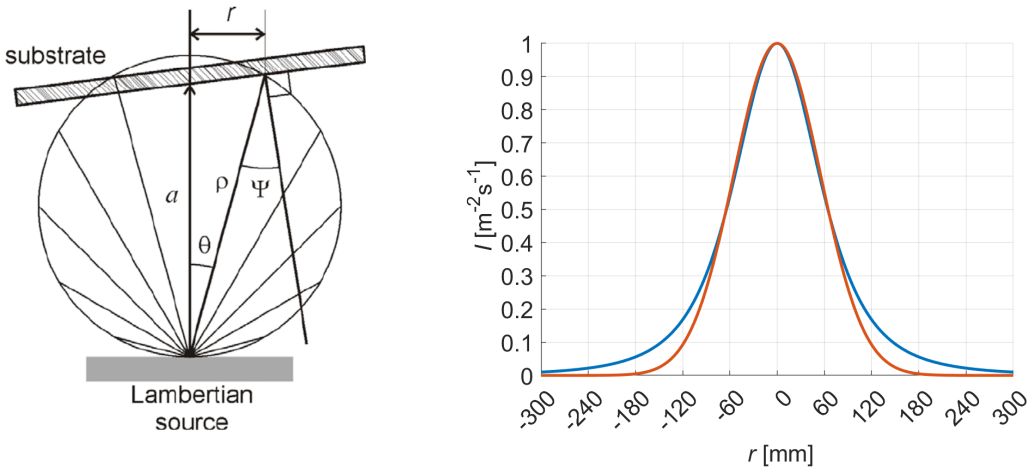

(a) (b)

Figure 3: a) Scheme of an emitting Lambertian source with a plane that the emitted atoms are deposited on. Adapted from [41]. b) Flux of an atomic beam emitted by an ideal effusion cell dependant on radial position. Blue line - according to theory [41], orange line - its Gaussian approximation.

Having the angular distribution of emitted atoms we can calculate the distribution of the atomic beam at a parallel to the pupil plane. For such a case, angle Ψ on the scheme 3a is equal to θ. We express the cosine in terms of the distance a from the source to the plane and the position r

$$\cos\theta = \frac{a}{\sqrt{a^2 + r^2}}. \tag{2.5}$$

From Knudsen's cosine law 2.4 we can get the flux per area

$$I(r) = \frac{\partial \Phi_\Omega}{\partial A} = \frac{aI}{\pi} \cos\theta \cos\Psi. \tag{2.6}$$

The area is given by the projection of the elemental area $\rho^2 d\omega$ onto the substrate at an angle of Ψ. Since $\theta = \Psi$ we can substitute to the above equation formulation 2.5 which gives us

$$\Phi\left(r\right) = \frac{aI}{\left(1 + \left(\frac{r}{a}\right)^2\right)^2}. \tag{2.7}$$

This equation is represented in Fig. 3b. It is often approximated using a Gaussian distribution also represented for comparison.

2.3 The nonequilibrium case

Not for every case ideal effusion cell can be applied. The assumptions we have stated are often not fulfilled which causes the impingement rate to be lower than in the ideal case. The described deviations are: the thickness of the pupil, the long distance between the evaporative material and the output, and the chance for a particle to evaporate from the material is below 1. To describe it we can apply the correction factor η, where

$$\eta = \frac{I_r}{I_\Omega}. \tag{2.8}$$

We can see the problem of the atomic beam passing through a pipe as electrons pass through a cable. Then the terms flow intensity, conductance and resistance are more familiar. Pressure difference resembles voltage. Similarly, a parallel of Ohm's law applies which in the atomic beam case can be represented as

$$I = C \cdot \Delta p, \tag{2.9}$$

where C is the conductance, the volume flow rate of a liquid through a vessel. We see that the correction factor η can be described by the conductance in the ideal configuration C_0 divided by the conductance in the real case C_r. Conductance for the molecular flow regime (assumption 2) is calculated as

$$C_0 = \frac{1}{4} a \bar{v}, \tag{2.10}$$

where $\bar{v}$ is the mean velocity. Let us now estimate the conductance for the real case. It will have three components. The first component represents that atoms are not always emitted from the material to the body's cell. It is regarded as the flow resistance between the liquid-vapour interface. It can be directly set by C_0 divided by the evaporation coefficient, an experimental constant. When atoms propagate through the effusion cell's tubed body, they can hit the walls and get attached to them. Conductance of pipes is estimated by the Clausing factor [42]. Clausing's theory proposes two regimes, of a short and long tube. We can call it short when its length l_p is smaller than 1.5 r_p, where r_p stands for the tube's cross-section radius. Then we can set the Clausing factor as

$$C_\mathrm{pupil} = \frac{C_0}{1 + \frac{l_\mathrm{p}}{2r_\mathrm{p}}}, \tag{2.11}$$

where r_p is the radius of the orifice. This is applied to the loss at the pupil. The cell's body is regarded as a long tube of length l_b where

$$C_\mathrm{body} = \frac{C_0 8 r_\mathrm{b}}{3 l_\mathrm{b} + 8 r_\mathrm{b}}, \tag{2.12}$$

where r_b is the body's radius. The conductance of the whole effusion cell C_r is calculated similarly to the conductance of serially connected wires

$$\frac{1}{C_r} = \frac{1}{C_\mathrm{material}} + \frac{1}{C_\mathrm{pupil}} + \frac{1}{C_\mathrm{body}}. \tag{2.13}$$

Now combing the definition of η with 2.9 and the expression for component conductances we obtain the correction factor as

$$\eta = \frac{8\alpha r_\mathrm{b} f}{8a((1+\alpha)f+\alpha) + \alpha(3f+4)l_\mathrm{b}}, \tag{2.14}$$

where f is the ratio between the radius of the pupil and the radius of the body . When we presume that one of the aspects is close to the ideal case we remove it from the formula. This loss is only for the output beam intensity from the effusion cell and does not affect its distribution. To give an example let us imagine an effusion cell of body length $l_\mathrm{b} = 1$ cm, cross-section $A = 2.0$ cm, pupil length $l_\mathrm{p} = 0.01$ cm, pupil's cross-section $a = 0.2$ cm, and vaporisation co-efficiency $\alpha = 0.9$. The pupil conductance will be $0.96C_0$ and the body's conductance will be $0.97C_0$ both of them can be approximated to the ideal case. The conductance between the material and the cell is described experimentally for every material. For silver, it is around $\alpha_\mathrm{Ag} = 0.9$ [43] and it is temperature-dependent. Since we can assume that the pupil and the body are close to an ideal case so only the evaporation coefficient remains which becomes the correction factor.

3 Behaviour of atoms in a MOT

This chapter presents a theoretical model of a 2D+3D MOT system, where atoms from an oven are first cooled by a 2D MOT and then ejected by a push beam to be trapped in a 3D MOT. T. G. Tiecke [28] introduced this model for lithium atoms. It estimates the oven flux, capture and cooling processes, and loss mechanisms. The model offers valuable insight into the inner workings of the setup, highlighting dependencies on various parameters. We present this model not only to enhance understanding of the MOT system but also as an alternative to simulations in providing guidance for designing experiments and estimating the trapping rate in the final trap. It is a semi-empirical model, which requires some of the elements to be measured.

3.1 From an oven to the 2D MOT

The model begins with an effusion cell of a pupil with an area a. It is regarded as an ideal case where the vapour pressure is expressed by 2.1. The intensity coming from the effusion cell is expressed by 2.3. The flux of the beam in terms of atomic

density $n_s = p_v/k_BT$ and mean velocity $\bar{v} = \sqrt{8k_BT/\pi m}$ is the atomic beam's intensity multiplied by the pupil area

$$\Phi_{\text{tot}} = \frac{1}{4} n_s \bar{v}\ a. \tag{3.1}$$

Atoms come directly to the 2D MOT from the pupil in the form of an atomic beam. Atoms will be trapped only if they go through the capturing area A_c and have a velocity below v_c. To calculate the trapping rate of the beam we sum all the atoms whose exit angle θ allows for going through the capture surface after distance l, and whose velocity is in the capturing range. We assume that atoms have Max-Boltzmann velocity distribution. This gives us a capture rate as

$$L_c = a n_s \int_0^{\Omega_c} d\Omega \frac{\cos\theta}{4\pi} \frac{1}{\mathcal{N}} \int_0^{v_c} v^3 \mathrm{e}^{-(\frac{1}{v_{\text{mp}}} v)^2} dv, \tag{3.2}$$

where a is the abundance of the regarded atom in the sample, $\Omega_c = A_c/l^2$ is the solid angle of capture, v_{mp} is the most probable atomic speed in the cell, and $\mathcal{N} = \frac{1}{4}\sqrt{\pi} v_{\text{mp}}^3$ is the normalisation factor of the speed distribution. For small angles, we can approximate cosine as unity so that the angular part will be simply $\frac{1}{4\pi}\Omega_c$. Assuming that the capture velocity is much slower than the most probable velocity we can set the exponent to 1 giving an easy integral to solve. The maximal theoretical capture rate is then

$$L_c \approx \frac{1}{2} a n_s A \left(\frac{v_c}{v_{\text{mp}}}\right)^2 \frac{\Omega_c}{4\pi} = \frac{1}{2} a \left(\frac{v_c}{v_{\text{mp}}}\right)^2 \Phi_\Omega, \tag{3.3}$$

where $\Phi_\Omega = \frac{\Omega_c}{4\pi}\Phi_{\text{tot}}$ is the flux of the beam emitted into Ω_c. We have used the relation $\bar{v} = \sqrt{\frac{4}{\pi}} v_{\text{mp}}$ between the mean and most probable velocity.

The only unknown factor is the capture velocity. We can take the model described in Chapter 1 to derivate it. We see the Zeeman trapping and Doppler cooling effect on an atom as a damped harmonic oscillator. Then the cooling time is $\tau \approx \beta/\kappa$. For an atom to be trapped the residence time has to be smaller than the cooling time. The time that the atom spends in the trap is mostly dependent on the speed in the 2D MOT-3D MOT axis, the direction in which there are no cooling beams. We can approximate the capturing velocity by the velocity it takes an atom to go to the trap in the cooling time

$$|v_c| \approx \frac{l}{\tau}. \tag{3.4}$$

3.2 Travel and capturing in the 3D MOT

After exiting the 2D MOT, the atomic beam goes through a tube to the 3D MOT. In this model, the pump beam is not considered. We can define the final loading

rate by the theoretical maximum trapping rate and an efficiency χ

$$L_r = \chi L_c. \tag{3.5}$$

It encapsulates the efficiency of trapping both MOTs by themself and the transfer efficiency χ_t between them. The transfer efficiency is related to the divergence of the beam. As discussed in Chapter 2.2 we can approximate the distribution at a position of the 3D MOT $l_{3\mathrm{D}}$ by a Gaussian profile of a 1/e radius R_G. The transfer efficiency is an integral over the normalised by $1/R_G$ distribution

$$\chi_t = 2\int_0^{\frac{R_a}{R_G}} \frac{1}{R_G^2}\left(1-\frac{r}{R_0}\right)\mathrm{e}^{-\left(\frac{r}{R_G}\right)^2} r dr, \tag{3.6}$$

where R_a is the acceptance radius, and R_0 represents the radius of the clipping area of the channel the atomic beam passes through. It is dependent on the divergence angle $\xi = R_G/l_a$. Note that it equals the transverse velocity ratio to the axial velocity, $\xi = v_t/v_z$. Additionally, we can introduce an acceptance angle $\alpha = R_a/l_a$, and a clipping angle $\omega = R_0/l_a$ into the above equation. After evaluating the integral we obtain

$$\chi_t(\bar{v}_z) = 1-(1-\frac{\alpha}{\omega})\mathrm{e}^{-(\alpha\bar{v_z})^2} - \frac{1}{2\omega\bar{v}_z}\sqrt{\pi}\ \mathrm{erf}(\alpha\bar{v}_z). \tag{3.7}$$

Since it is velocity dependant we have to calculate the velocity-averaged transfer efficiency by

$$\chi_t(\bar{v_z}) = \int_0^{v_c} \chi_t(\frac{v_z}{v_t})\phi(v_z)dv_z, \tag{3.8}$$

where $\phi(v_z)$ is the normalised axial velocity. In an experimental setup, it is set by fluorescence detection.

3.3 Loss of atoms

Discussed efficiency doesn't provide any notion of how the collisions affect the trapping rate. Moreover, the provided model doesn't include loss due to the fall into the dark state. Since the full flux coming from the effusion cell is much bigger than the small part that can be trapped in the 2D MOT we expect the cold flux coming from the 2D MOT Φ_c to be diminished by 'knock-out' collisions. They take place in the part of the beam which is the densest - the first few centimetres after the effusion cell. Let us calculate the collision rate of an atom moving at velocity v_c along the x-axis. Atom is at a position l from the oven and the angle $\theta_0(l)$ describes the biggest angle that an atom can have at this position if it was emitted from the pupil of radius r_p. The majority of atoms are much hotter than the cold fraction so $\bar{v} \gg v_c$. Loss of the flux can be expressed by

$$\dot{\Phi} = \frac{1}{2}\sigma_6 n_s \int_0^{\theta_0(l)} v_r \sin\theta d\theta, \tag{3.9}$$

where σ_6 is the collision cross-section, angle $\theta_0 = \arctan(r_\mathrm{p}/l)$, and $v_r \approx \bar{v}$ is the relative velocity of the colliding atoms. Solving this differential equation

$$\Phi(l) = \Phi_c \exp\left[-\frac{1}{2}\sigma_6 n_s \frac{\bar{v}}{v_c}\int_0^l (1-\cos\theta_0 dx)\right]. \tag{3.10}$$

We can substitute $\cos\theta_0 = x/\sqrt{x^2+r_\mathrm{p}^2}$ and substitute l with infinity since it is much larger than the size of the pupil. Then the integral is $\int_0^\infty \left(1 - x/\sqrt{x^2+r_\mathrm{p}^2}\right) dl$ have two terms that diverge but the infinities can be subtracted yielding r_p as the result leaving the final attenuated flux due to collisions as

$$\Phi_\mathrm{col} = \Phi_c \exp\left(-\sigma_6 n_s \bar{v}\tau_6\right). \tag{3.11}$$

Variable $\tau_6 = r_\mathrm{p}/2v_c$ is the time of the attenuation process. The only unknown is σ_6. The influence of hot atoms on the cold elements is through the Van-Der Waals force. When hot flux travels close to the slower atoms it exchanges momentum with them resulting in a knock-out. The difference in velocity between those groups of atoms is large so the fast atoms are not affected by this interaction. To calculate the change of momentum we integrate the transverse component of Van der Waals force

$$\Delta p = \frac{1}{2}\int_{-\infty}^{+\infty} F_\perp(r) dr. \tag{3.12}$$

To model the force we will use London's dispersion interaction between two neutral atoms [44]. According to it the potential is $U(r) = Cr^{-6}$ and the derivative over the distance r gives the force. The Bohr radius and the Hartree energy describe the constant as $C = 1389 a_0^6 E_h$. Hartree energy E_h represents the electrostatic potential energy between two electrons separated by a distance of 1 Bohr. The time t is expressed with the angle θ and the distance of the closest approach $b = r\cos\theta$. Combining it with the equation 3.12 and solving the integral gives us

$$\Delta p = \frac{15\pi C_6}{16\bar{v}b^6}. \tag{3.13}$$

We can assume that a small momentum transfer of $\Delta p_\mathrm{min} = 0.1 m v_c$ can result in a knockout of the atoms from a capture angle. With this assumption being inserted in the above equation, the collision's cross-section will be a circular area defined by the distance of the closest approach

$$\sigma_6 = \pi b_6^2 = 3.2\sqrt[3]{\frac{C_6}{m v_c \bar{v}}}. \tag{3.14}$$

We have considered losses through atom's interaction along the path to the 2D MOT but also in the traps themselves atoms are knocked out due to the resonant collisions. This is a quantum effect that is prevalent in cold gases. Resonant collision is known as interaction when not only the kinetic energy is transferred from one atom to another but so is its internal energy. In such a case, the minimum momentum transfer value needed for any atom to be knocked out from the trap is $\Delta p_{\min} = m v_c$. We can repeat the process as for scattered atoms but with an approximation by [45] $F(r) = 3C_3 r^{-4}$, where $C_3 = e^2 a_0^2 / 4\pi\varepsilon_0 \cdot D_{eg}^2$. The constant D_{eg} is the transition dipole moment, specific for any transition we are modelling. For potassium, and caesium, they can be found at [31] and for silver at [46]. Analogously to the previous part, we obtain an expression of the cross-section of the interaction [47]

$$\sigma_3 = \sqrt[3]{\left(\frac{e^2 a_0^2 D_{eg}^2}{2\pi\varepsilon_0}\right)^2}. \tag{3.15}$$

Combining all the elements that we have obtained we get the final equation describing the trapping rate in the 3D magneto-optical trap

$$L_{3D} = \bar{\chi}_t a_N n_s \bar{v} A \left(\frac{v_c}{\alpha}\right)^4 \frac{\Omega_c}{8\pi} \exp\left[-n_s \bar{v}(\sigma_6 \tau_6 + \sigma_3 \tau_3)\right], \tag{3.16}$$

where $\tau_3 = A/4\pi l^2 \cdot \tau_{\text{res}}$. Time τ_{res} is the residence time in the trapping beams.

It is a fully computational method that takes into account interactions between atoms. However, it has many assumptions and approximations, and it still needs experimental measurements and a great deal of knowledge about the system. It can be used for modelling solely a pre-existing setup since it would be difficult to design and predict a completely new system with this technique.

4 Simulating atoms in magneto-optical traps

Magneto-optical traps constitute a universal spectroscopic tool. The ability to create relatively cold atoms allowed for research on the photoassociation of homonuclear caesium [48] or potassium [49] molecules or heteronuclear molecules such as KRb [50]. The available experimental data allow for the estimation of the interaction potentials between these atoms, which is important in obtaining ultracold molecules in the ground state. In previous chapters, we described MOTs, how they work, and what influences their efficiency. We start this chapter with an introduction of essential information about caesium, potassium and silver which will be used in the simulation. In the next sections, we will present what open source packages are available for simulating atoms and how our program is structured.

4.1 Properties of caesium, potassium and silver

4.1.1 Caesium

Caesium has the chemical symbol Cs and its atomic number is $Z = 55$. It is an alkali metal, which means that it has a single electron on its outer-orbital - s-orbital. Due to this characteristic, all alkali metals have similar properties. A single electron on the outer orbital makes the element highly chemically reactive, since the ionization energy of the electron is low. All information has been taken from [36].

Table 1: Characteristic properties of the only isotope of caesium. Its atomic number A, number of neutrons N, abundance in nature, atomic mass, and spin quantum number I.

A	N	Abundance [%]	m [u]	I
133	78	100	38.96	3/2

Caesium has a single stable isotope represented in Tab. 1.

Table 2: General properties of Caesium.

Property	Value
Melting point	301.59 K
Boiling point	944 K
Density at 293 K	1.93 g/cm^3
Vapour pressure at 298 K	$1.3 \cdot 10^{-8}$ mbar
Electronic structure	[Xe] $6s^1$

Caesium has a vapour pressure given in atmospheric pressure by [39]

$$\log(p_{\text{solid}}) = 4.711 - 3999 \cdot T^{-1} + C \log T + D \cdot T^{-3} \quad 298K < T < 337K \quad (4.1)$$

$$\log(p_{\text{liquid}}) = 4.165 - 3830 \cdot T^{-1} \quad 337K < T < 550K. \quad (4.2)$$

Caesium's cooling transition is the D2 line with properties showed in 3.

Table 3: Characteristic values of a D2 line for caesium. Its wavelength λ, natural linewidth $\Gamma/2\pi$, lifetime of excited state τ, saturation intensity I_{sat}, and the Doppler cooling temperature limit T_D.

	^{133}Cs
λ [nm]	852.347
$\Gamma/2\pi$ [MHz]	5.223
τ [ns]	30.473
I_{sat} [mW/cm^2]	1.654
T_D]μK]	125

4.1.2 Potassium

Potassium has the chemical symbol K and its atomic number (number of protons in the nuclei) is $Z = 19$. All the information has been taken from [51].

Table 4: General properties of potassium.

Property	Value
Melting point	336.8 K
Boiling point	1047.15 K
Density at 293 K	0.862 g/cm^3
Vapour pressure at 293 K	$1.3 \cdot 10^{-8}$ mbar
Electronic structure	[Ar] $4s^1$

Potassium has three stable isotopes represented in Tab. 5. Two of them are bozons (^{39}K and ^{41}K) and one is a fermion ^{40}K. Their general properties are common and shown in Tab. 4.

Table 5: Characteristic properties of potassium's stable isotopes. Their atomic number A, number of neutrons N, abundance in nature, atomic mass, and spin quantum number I.

A	N	Abundance [%]	m [u]	I
39	20	93.26	38.96	3/2
40	21	0.01	39.96	4
41	22	6.73	40.96	3/2

Potassium has a vapour pressure given in atmospheric pressure by [39]

$$\log(p_{\text{solid}}) = 4.961 - 4646 \cdot T^{-1} \tag{4.3}$$

$$\log(p_{\text{liquid}}) = 4.402 - 4453 \cdot T^{-1}. \tag{4.4}$$

It is important when calculating flux coming from the surface of a background gas. If we simulate flux coming from an effusion then additionally we need to know its evaporation coefficient. For potassium it is $\alpha = 0.08$ at $T = 1200$ K [52].

Table 6: Characteristic values of a D2 line for different isotopes of potassium. Its wavelength λ, natural linewidth $\Gamma/2\pi$, lifetime of excited state τ, saturation intensity I_{sat}, and the Doppler cooling temperature limit T_D.

	^{39}K	^{40}K	^{41}K
λ [nm]	766.701	766.701	766.700
$\Gamma/2\pi$ [MHz]	6.035	6.035	6.035
τ [ns]	26.37	26.37	26.37
I_{sat} [mW/cm^2]	1.75	1.75	1.75
T_D [μK]	145	145	145

Potassium's strongest spectral lines of the ground state are D1 $\left({}^2S \rightarrow {}^2P_{1/2}\right)$ and D2 $\left({}^2S \rightarrow {}^2P_{3/2}\right)$. Those are common lines for alkali metals. The D2 line, which parameters are put in Tab. 6, is used for cooling. For cooling atoms, it is crucial to take into account their hyperfine structure since they don't have a closed transition. Due to the hyperfine structure, an excited electron can fall into a level not accessed by the light, stopping the cooling processes. This so-called "dark state" needs to be accessed by an additional, typically weaker, laser beam called a repumping beam (repump). The force exerted upon the atoms is dominated by the cooling light, tuned to an almost closed transition. The repumping light is mainly needed to counteract the hyperfine optical pumping in the ground state, consequent to off-resonant excitation. This is different for bosonic potassium. The spacings in hyperfine $4^2P_{3/2}$ level are comparable to the natural linewidth. In this case, the cooling transition $\mathrm{F} = 2 \rightarrow \mathrm{F} = 3$ is not closed since the $\mathrm{F} = 1, 2$ states are excited with similar rates. This needs to be addressed by a fairly intense repumping light which makes it in practice a second cooling beam.

4.1.3 Silver

Silver has the chemical symbol Ag and its atomic number is $Z = 47$. It is a transition metal. Silver, compared with other alkali metals has high electronegativity which allows for a large electric dipole moment when part of a molecule. Making it a promising component for polar molecules [18].

Table 7: Characteristic properties of silver's stable isotopes. Their atomic number A, number of neutrons N, abundance in nature, atomic mass, and spin quantum number I.

A	N	Abundance [%]	m [u]	I
107	60	46	38.96	3/2
109	62	53	40.96	3/2

Silver has two stable isotopes represented in Tab. 7.

Table 8: General properties of silver [53].

Property	Value
Melting point	1234.93 K
Boiling point	2435 K
Density at 293 K	10.49 g/cm^3
Vapour pressure at 293 K	$1.4 \cdot 10^{-41}$ mbar
Electronic structure	[Kr] $4d^{10}$ $5s^1$

Silver has a vapour pressure given in atmospheric pressure by [39]

$$\log(p_{\text{solid}}) = 9.127 - 14999 \cdot T^{-1} - 0.7317 \cdot \log T \quad 337K < T < 550K \tag{4.5}$$

$$\log(p_{\text{liquid}}) = 5.752 - 13827 \cdot T^{-1} \quad 337K < T < 1600K. \tag{4.6}$$

Silver's evaporation coefficient is $\alpha = 0.9$ at $T = 830$ K [43].

Table 9: Characteristic values of the cooling transition for silver. Its wavelength λ, natural linewidth $\Gamma/2\pi$, and saturation intensity I_{sat}.

	^{109}Ag
λ [nm]	328.1
$\Gamma/2\pi$ [MHz]	23.4
I_{sat} [mW]	870

The proposed cooling transition is $4d^{10}5s^2S_{1/2} \rightarrow 4d^{10}5s^2S_{3/2}$ described in Tab. 9 [54]. Silver is not as well documented as potassium or caesium so we have less information about its energy structure.

4.2 Open-source software packages for atom trajectory simulation

Let us consider a ^{109}Ag atom in a standard, six-beam magneto-optical trap (of a cooling and repumping frequency). We would like to calculate its movement in the trap. We can use the previously described OBE. For a ^{109}Ag atom that has 48 Zeeman states the OBE would constitute a total of $48^2 = 2304$ coupled, first-order, time and position-dependent differential equations for the atom's internal states (plus an additional 6 differential equations to account for its classical motion). We see that performing an efficient simulation that allows for quick solutions of the equations is needed. Since we would like to simulate multiple systems where we need to iterate over multiple time steps we need a solution that will be most

importantly time and processing-efficient. We have presented all the knowledge on which we base our theoretical model, which allows for a discussion about the setup. In this chapter, we go through two open-source tools used for laser cooling simulation: PyLCP and AtomECS. We describe why we have used the AtomECS, how it was used, what were its limits, how we surpassed some of them, and what other scripts we created to obtain our final procedure.

4.2.1 PyLCP

PyLCP is an open-source Python package created for laser cooling physics [55]. It can calculate the trajectories of atoms or molecules in arbitrary laser and magnetic fields. With a provided Hamiltonian the program solves optical Bloch equations, integrates them and generates equations of motion for the particles. It has been tested against well-known results [55]. It can calculate atom's movement using OBE, rate equation method or a heuristic equation which comes from direct application of the equation 1.42. Moreover, it can include a multi-level structure of the atom and bi-chromatic traps.

It is a powerful tool but to determine if it is suitable for our case we need to go through the architecture of the programming language. Python has an object-orientated programming (OOP) architecture. The OOP is based on objects that have attributes with which we can interact by using methods. To create an object we need a class that connects all of the mentioned components. Each time we create an object it is saved in an arbitrary place in memory with information about its methods. When we scale a system by adding millions of more objects repeated memory about their methods becomes significant. Furthermore updating those objects will be time-consuming since we have to access the memory at random points. Additionally, arbitrary memory position makes parallel computing more difficult. This makes OOP a poor decision if we want to simulate an atomic source that emits thousands of millions of objects.

4.2.2 AtomECS software

AtomECS [56] is an open-source Rust package created for simulating magneto-optical trap and Zeeman slower. It is implemented using an entity-component system (ECS). It is a programming architecture, where entities are integers identifying objects (atom 1, atom 2 etc.), it has components which define its characteristics (for example position component would keep X, Y, and Z coordinates) and systems that process entities (for example takes the component of positions, and velocities and changes the positions of all the entities based on the time step and velocity). This allows all the components to be listed in a single place in memory and when a system is invoked it goes through all of them saving time and allowing parallel computing. Additionally creating new objects doesn't take any additional memory besides the one we give as its components. This makes ECS a natural programming architecture to use for the simulation of atoms in MOT and that is why we picked it above the PyLCP Python package.

4.2.3 Abilities and limits of AtomECS

In AtomECS simulation we place different entities inside a simulation world, for example, laser beams, magnetic field, and atoms. We can define their different components. AtomECS simulates the movement of the atoms by calculating the force described in section 1.6. For that, it calculates the detuning based on the atom's position and velocity relative to laser beams and magnetic field. The magnetic field can be inserted as a quadrupole field or as an explicitly defined value on a 3D grid. AtomECS supports different types of sources as an oven with a 3D Maxwell-Boltzmann distribution with a Lambertian spread of the intensity. Additional elements that can be added are: an upper-velocity limit for simulated atoms, fluctuations in the scattering force, loss of atoms due to relaxation to a dark state, and simulation volumes to limit the space atoms can go through. The script gives back the subsequent atoms' positions and velocities in a .txt file.

The transition that we would like to use for cooling has to be addressed at the beginning of the simulation. It will be the only transition for this system that the cooling will be regarded for. The software recognizes atoms as two-level structures so it does not regard the scattering on different levels, which could lead to heating. This also makes it difficult to simulate multiple species at the same time, and take into account different colour traps or repumping beams.

Limitations of the AtomECS include:

1. the magnetic field evolves infinitely with a linear dependence on position;
2. simulated volume affects purely atoms so it is not possible to shape the beam's profile by it;
3. simulation provides only the trajectories of atoms and doesn't include any further calculations;
4. software has an intrinsic limit on how far away from a laser beam atoms can be inserted into the simulation;
5. cooling forces are calculated only for one transition per simulation.

4.2.4 Introduced changes

With the described limits inherent to the AtomECS, it is impossible to simulate a 2D MOT and a 3D MOT where a push beam transfers atoms. A magnetic field from both traps will influence both of them. The push and counter-push beams won't be shaped by the spaces they propagate exerting force on the atoms through the whole length of the system. Moreover, it is not possible to create atoms far away from the beams and the software does not simulate two-colour traps. To perform designed simulations we have addressed those problems.

In the AtomECS script, we have modified the quadrupole component, so that it will shape the magnetic field to decrease to 0 outside the trapping range. We have

added a mask with an adjustable radius for a Gaussian beam. It will set intensity to 0 as if it was modulated by an iris or a pipe. We have added a specific entity that will modify the simulation space allowing for limitless positioning of atoms relative to the laser beams. We have also created a solution for a simulation of traps of different colours. We created a script that will perform a simulation of the first trap of a single colour, then when it calculates and saves all the trajectories, a second simulation will be initiated by inserting atoms from the saved file and simulate a second trap of the second frequency.

The last limit remains which is the lack of possibility to simulate the effect of the repumping beam or two-colour cooling. This won't be considered in the forthcoming simulations.

4.3 Simulation scheme

4.3.1 Calculating atomic movement

In this section, we will go through the basis of simulation using the AtomECS package on an example of a novel 2D+ 3D MOT system for caesium atoms. The script was written by us analogically to the examples provided on the AtomECS GitHub page [57].

```
        let now = Instant::now();

        let mut sim_builder = SimulationBuilder::default();
        sim_builder.add_plugin(LaserPlugin::<{BEAM_NUMBER}>);
        sim_builder.add_plugin(LaserCoolingPlugin
            ::<Silver109_328,{BEAM_NUMBER}>::default());
        sim_builder.add_plugin(AtomSourcePlugin
            ::<Silver109>::default());
        sim_builder.add_plugin(FileOutputPlugin::<Position, Text, Atom>
            ::new("pos.txt".to_string(), 100));
        sim_builder.add_plugin(FileOutputPlugin::<Velocity, Text, Atom>
            ::new("vel.txt".to_string(), 100));
        let mut sim = sim_builder.build();
```

First, we start measuring the time the simulation takes, by initialising structure `Instant`, a saved point in time. Next, we create a simulation builder which is a structure that follows a pattern in building a simulation. We insert additional plug-ins which are external parts of the code that allow for specific calculations or saving the results in a .txt file. We specify how many laser beams we will simulate, what transition will be used for cooling and what kind of atomic species will be cooled. Information about the atom and its transition is saved as an entity where we add specific characteristics.

```
            species!(Cesium133, Cesium133_852D2, 133);
            transition!(
                Cesium133_852D2, //
                351_725_718_500_000.0, // 4 2S1/2 - 4 2P3/2 transition
                5.22e6, // Natural Line Width
                11.0, // Saturation intensity in W/m^2 = 10*mW/cm^2
                1.33*BOHRMAG, // Shift of the sigma+ transition in magnetic field
                -1.33*BOHRMAG, // Shift of the sigma- transition in magnetic field
                0.0 // Shift of the pi transition in magnetic field
            );
```

We obtain a fully configured simulation object `sim`. The command `let mut` creates an object that can be changed after initialisation. Before adding entities we need to introduce non-mutable 23 parameters of the system. They will be part of the components defining all the entities and will be visible in the next parts of the script as names of the physical properties, for example `quadrupole_gradient_2d`.

```
        sim.world.insert(ApplyGravityOption);

        sim.world
            .create_entity()
            .with(QuadrupoleField3D::
            gauss_per_cm(quadrupole_gradient_2d, Vector3::x()))
            .with(Position {pos: Vector3::new(0.0, 0.0, shift_z * 0.001)})
            .build();

        sim.world
            .create_entity()
            .with(QuadrupoleField3D::
            gauss_per_cm(quadrupole_gradient_3d, Vector3::z()))
            .with(Position {pos: Vector3::new(distance * 0.001, 0.0, 0.0)})
            .build();
```

The first system that we introduce is `ApplyGravityOption`. It will add a gravitational force in the $-Z$ direction to every entity with mass. The next step is to create a structure of a quadrupole magnetic field. We specify the gradient (in G/cm), symmetry axis, and position of the centre (in m). The coordinate system is defined where the z-axis faces upwards, against the direction of gravity and the x-axis is aligned with the direction of the atomic beam outgoing from the 2D MOT. The system updates the grid of the magnetic field using the `calculate_field` function. It was modified to decrease with the position outside the trap to 0. This is not a physical approximation since the magnetic field outside the trap is described by integral equations [58]. With such a magnetic field atoms in a laser

light would experience the Zeeman slowing. To ease the calculations we decided to approximate that it falls directly to 0.

```
            pub fn calculate_field(
                pos: Vector3<f64>,
                centre: Vector3<f64>,
                gradient: f64,
                direction: Vector3<f64>,
            ) -> Vector3<f64> {
                let delta = pos - centre;
                let x = delta[0];
                let y = delta[1];
                let z = delta[2];
                let z_comp = delta.dot(&direction) * direction;
                let r_comp = delta - z_comp;
                if (x*x + y*y + z*z).sqrt() > 0.1 {
                    0.0 * gradient * (r_comp - 2.0 * z_comp)
                } else {
                    gradient * (r_comp - 2.0 * z_comp)
                }
            }
```

Next, we add laser beams. We present an example of the code with a beam that is part of the 2D MOT. Added components are the position of the centre at its smallest waist `Intersection`, 1/e radius, power (in W), direction, Rayleigh range, and ellipticity. Ellipticity is defined as

$$\epsilon = \sqrt{1 - \frac{r^2}{R^2}}, \tag{4.7}$$

where R and r are the big and small radius of the beam. Rayleigh range has been set to infinity for every beam except the push beam since it interacts at a long enough distance that its divergence cannot be neglected. Its Rayleigh range was calculated by

$$z_\mathrm{r} = 2\pi \frac{r_{1/e}^2}{\lambda}, \tag{4.8}$$

where waist has been substituted by the 1/e radius $w_0 = 2/\sqrt{2} \cdot r_{1/e}$. As this beam will have to interact with atoms we need to add component `CoolingLight` holding information about laser cooling: transition, detuning, and polarisation.

```
            sim.world
                .create_entity()
                .with(GaussianBeam {
                    intersection: Vector3::new(0.0, 0.0, shift_z *
                    ↪  0.001),
```

```
                    e_radius: radius_2d * 0.001 / 2.0_f64.sqrt(),
                    power: power_2d * ratio_power_3d_2d * 0.001 / 2.0,
                    direction: Vector3::new(0.0, 1.0, 1.0).normalize(),
                    rayleigh_range: f64::INFINITY,
                    ellipticity: ellipticity,
                })
                .with(CoolingLight::for_transition::<Cesium133_852D2>(
                    detuning_2d,
                    1,
                ))
            .build();
```

For a push beam, we can add component `CircularMask` which has been modified so that by providing the radius of the mask we modify the beam profile to cut away an outer ring, as if done by an iris. We created such an entity 11 times for 6 3D MOT beams, 4 2D MOT beams and one push beam, where the detuning, polarisation, and direction were adjusted respectively. The next step in the simulation-building process is to add atoms. We can do it by placing atoms one at a time with specified positions and velocities, creating an effusing surface, placing an atomic beam, and lastly with an oven. The oven simulates only its orifice so we specify only its characteristics.

```
            sim.world
            .create_entity()
            .with(
                OvenBuilder::<Cesium133>::new(
                    temperature,
                    Vector3::new(0.0, 0.0, -1.0).normalize())
                    .with_aperture(OvenAperture::Cubic { size:
                    ↪  [radius_2d * 0.001 * 2.0, small_radius*2.0,
                    ↪  thick * 0.001]})
                    .build(),
            )
            .with(Position {
                pos: Vector3::new(0.0, 0.0, small_radius),
            })
            .with(MassDistribution::new(vec![MassRatio {
                mass: 133.0,
                ratio: 1.0,
            }]))
            .with(AtomNumberToEmit {
                number: number_to_emit_s,
            })
            .with(ToBeDestroyed)
            .build();
```

Components that have to be specified are position, shape, volume, direction,

temperature (in K), atomic species, ratio, and how many atoms it emits. The ratio is the probability of emitting this particle. We can introduce abundance at this point if we are modelling a natural sample and atom with more than one stable isotope, but in this example, caesium is the only stable isotope. Lastly, we add a component `ToBeDestroyed`, which marks this entity that it should be deleted after the first iteration. This component is specific to ovens, as we simulate a group of atoms emitted simultaneously, rendering the oven redundant in the next time steps. Atoms can be also emitted at a specific rate using `EmitNumberPerFrame`. To model the background gas as an atomic source we have set 6 ovens as emitting surfaces around the cooling volume of the trap according to the model of [21]. Every oven was set to emit towards the centre.

```
            let dir = Vector3::new(1.0, 0.0, 0.0).normalize();
            let perp_x = dir.normalize().cross(&dir);
            let perp_y = dir.normalize().cross(&perp_x);

            sim.world
            .create_entity()
            .with(Position {
                pos: Vector3::new(0.06, 0.0, shift_z * 0.001),
            })
            .with(Cylinder {
                radius: 0.00075,
                length: 0.02,
                direction: dir,
                perp_x: perp_x,
                perp_y: perp_y
            })
            .with(SimulationVolume {
                volume_type: VolumeType::Inclusive,
            })
            .build();
```

We have provided all the main components of the cooling setup. Now we need to add boundaries that will delete outlying particles saving computational time. It is a simple entity with an additional `SimulationVolume` component. It can be either `Inclusive` or `Exclusive`, which determines if the system deletes atoms that go inside the volume or escape it. We create a simulation volume for the source and the science chamber, a connection between them, and a differential pumping tube. Additionally, by adding and adjusting the simulation volume components, we create apertures that shape the atomic beam. In this example, we have a volume shape as a `Cylinder` for which we had to define the symmetry axis to be the x-axis.

```
            sim.world.insert(VelocityCap { value: velocity_cap });

            sim.world.insert(Timestep { delta: 1.0e-6 });

```

```
            sim.world.insert(ApplyGravitationalForceSystem);

            for _i in 0..(time * 1000) {
                sim.step();
            }

            println!("Simulation completed in {} ms.",
             ↪  now.elapsed().as_millis());
```

At the end of the script, we add `VelocityCap` (in m/s), which is a component that in the first frame deletes all the atoms that have velocity below the set value. It is advised to do so since it saves a great deal of computational power. Doing so doesn't influence the results because the simulation doesn't consider atom-atom collisions and, an atom has to have a low kinetic energy to be trapped. To evaluate the system in time we add a loop that iterates the simulation by a predefined time step.

4.3.2 Trajectory analysis

For calculating the system's characteristics, we compared Matlab, Rust, and Python as possible programming environments. Rust would be the fastest due to its scalability and efficient memory management, but Python was used because we had the most experience in it since it is the most popular programming language used in laboratories to analyse data and control devices. Moreover, the speed difference with Rust wouldn't be substantial in this case. In this section, we will explain our Python script that calculates the flux based on the trajectories using the theoretical model described in section 2.2 and give the velocity distribution after the 2D MOT. Files are CSV tables converted from the .txt files. In a single row, there is a label and the three components of the atom's position (or velocity). Subsequent iterations are saved by repeating the labels with updated values. First, we filter out the iterations that don't contain any atoms. The next step is to take only the atoms that have got out from the 2D MOT, so their position in the x-axis has crossed the whole trap chamber and the tube leading to a science chamber. This decreases greatly the computational time in the next steps. To measure the velocity distribution at a specific X position we check at which time the atom has been cooled down by the 2D MOT and then how much time it took to cross the position X. We divide the distance from the centre of the 2D MOT to X, by the time obtaining the mean velocity of the atom. We distinguish the atoms trapped in the 3D MOT by checking which atoms have their final velocity below a set threshold and have not left the simulation volume. The threshold is set to be far smaller than the mean value of the velocity distribution of atoms outgoing from the 2D MOT. Next, we determine the efficiency of trapping as the ratio of the trapped atoms to the number of all atoms considered (including atoms whose velocity was above the velocity cap). If the atomic source is an oven we calculate the flux according to the model 2.3 discussing its Clausing factors. If it is a background gas we calculate using the impingement rate.

4.3.3 Optimisation

For the optimisation, we use Matlab as it has a developed function that does Bayesian optimisation `bayesopt()`, it is easier to visualize 3D data, and a basic example was provided in the AtomECS GitHub repository. We define the time we want the optimisation to take and an evaluation variable. The function will be tasked with decreasing the evaluation variable. We need to deliver limits for the parameters and initial values that we believe should provide a decent result. An additional version of the Rust script had to be created that imported values of the parameters from a separate file. This allowed exchange between Matlab and Rust scripts.

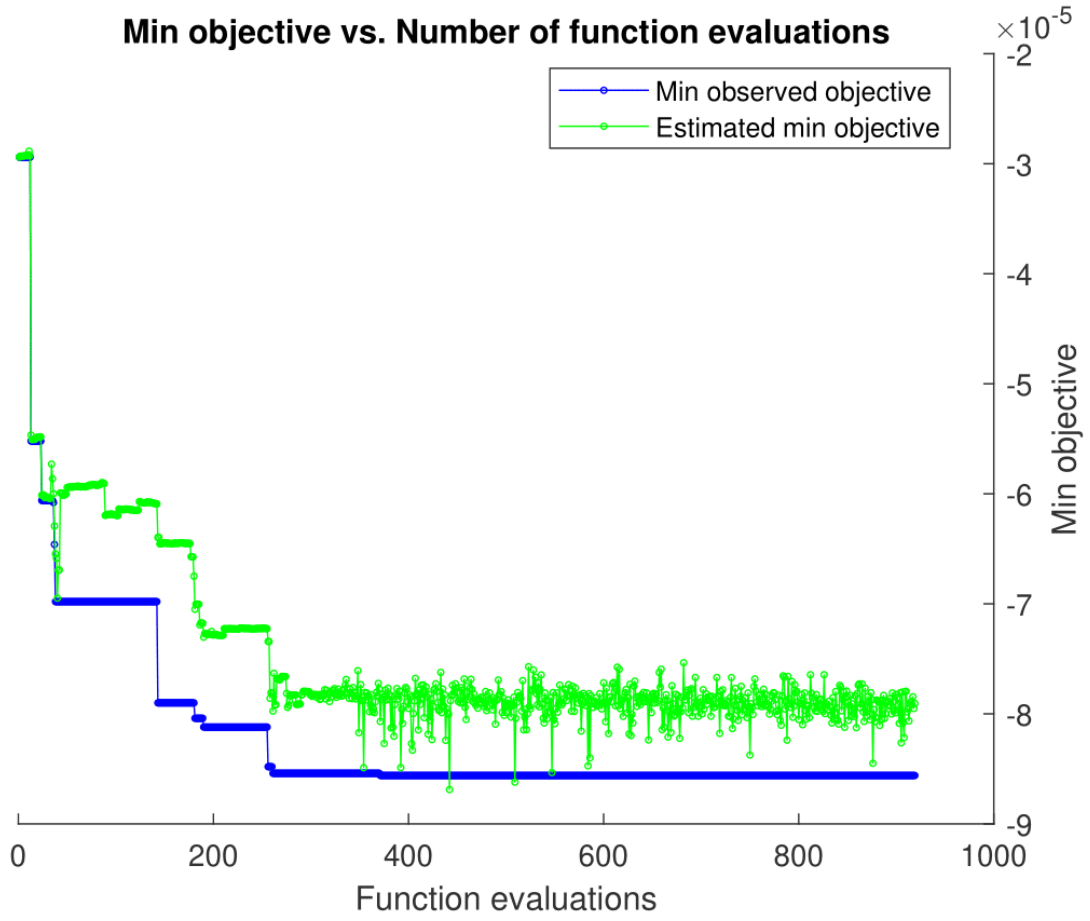

Figure 4: Negative of trap efficiency as a function of optimisation script iterations. The green line represents the calculated value and the blue line shows the lowest achieved by the function throughout the optimisation time. This optimisation performed for seven hours and optimised values for 6 parameters.

Next, it was crucial to establish a scoring variable that would decrease only in the case of trapping atoms in the 3D MOT. For example, the first proposed score was the negative number of atoms that passed through a plane just before the 3D MOT but didn't pass the distance afterwards. In the process of optimisation, such scoring encouraged a combination of parameters for the laser beams that

deflected the atoms to the side. For this reason, atoms were also filtered to have a velocity below 0.3 m/s, a value far below the velocities of the atomic beam distribution. This additional constraint made the optimisation to propagate a solution where atoms were trapped and cooled. Fig. 4 presents how the algorithm, by changing the parameters around the lowest achieved result (blue line), obtains a lower evaluation score with every iteration (green line).

5 Proof of concept

As shown we have established a theoretical model capable of simulating and optimising an MOT system. Before applying it to a new setup we have to check to what level this model can be trusted. For this reason, we have simulated three different documented experiments one for each species we will be working on. Simulations have been performed using all the information in the articles and thesis connected to the research. In the descriptions of the experimental setups, we have included information solely relevant to the simulation. Elements, like a probing beam used for spectroscopy of the atoms, are not mentioned.

5.1 Caesium

We would like to perform the first verification of our simulation, using experimental data from Aden Lam's apparatus dedicated to the formation of ultracold sodium-caesium [22] [59]. In this experiment, caesium atoms are cooled in a 2D-MOT - push beam - 3D-MOT configuration, similarly to the configuration that will be implemented in our newly created experiment

5.1.1 Experimental setup

The sources of caesium are dispensers which, when heated, effuse atoms. Dispensers are embedded near the trap centre. They create a caesium vapour which, as explained in section 2.1, can be obtained at room temperature. The vapour pressure in the glass cell is in the 10^9 torr range.

Table 10: We present characteristics crucial for the simulation of the documented experimental setup of a 2D+3D MOT for caesium atoms. We include wavelength λ, radius R, power P and detuning δ for lasers that create the traps and the push beam (denoted by '+'), the gradient of used magnetic fields ΔB, and the distance d between the centres of the two traps. Every laser beam shares the same detuning.

Parameters	Value
d [mm]	610
λ [nm]	852
R_{2D} [mm]	34x8
R_{3D} [mm]	6.9
R_{+} [mm]	2.2
P_{2D} [mW]	150
P_{3D} [mW]	10-20
P_{+} [mW]	3
δ [Γ]	-1.9
∇B_{2D} [G/cm]	13
∇B_{3D} [G/cm]	13

In a glass vacuum chamber two retro-reflected beams create a Doppler cooling region and two electromagnets in the anti-Helmholtz configuration create a magnetic gradient trapping the atoms in the X, and Y axes, as defined in Fig. 5. The beams creating a 2D MOT are elliptical so we describe their size by the major radius R_{2D} and ellipticity defined as

$$\epsilon = \sqrt{1 - \left(\frac{r_{2D}}{R_{2D}}\right)^2}, \tag{5.1}$$

where r_{2D} is the minor radius. For the purpose of this thesis, radius will describe the major radius of an ellipse. Two smaller and less intense beams are introduced as push and counter-push using a 45° mirror inside the glass cell. Through the mirror, a hole serves as an escape output for the atomic beam and a differential pumping tube. The pressure differential between the glass cell and science chamber is 10^{-3}, enabling a pressure of 10^{-11} Torr in the science chamber at 10^{-9} Torr in the 2D MOT region.

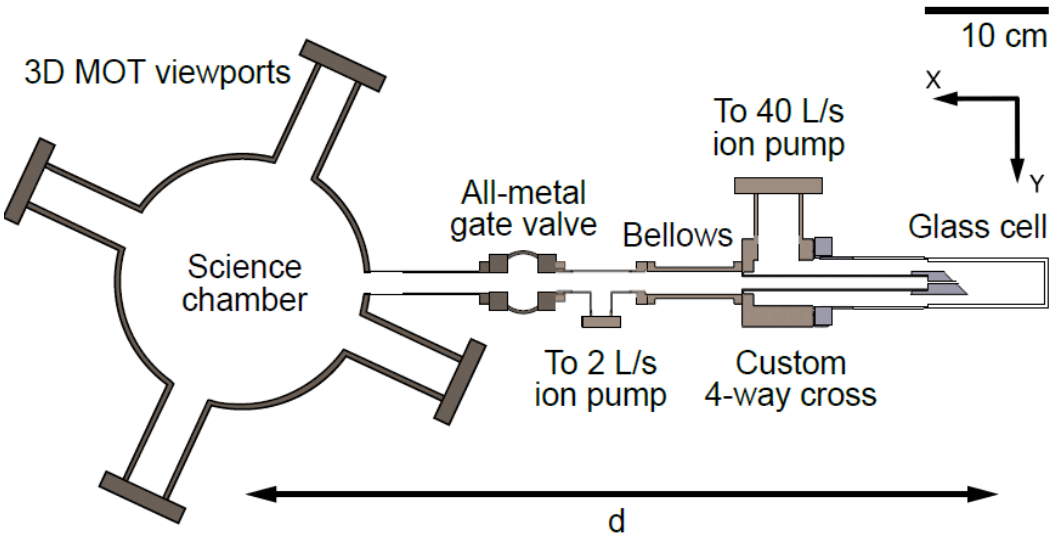

Figure 5: Scheme of Aden Lam's experimental setup. Accommodated from [22] with a modified coordinate system to match the one of simulation.

The ratio between the counter-push and push beams is adjusted to propel atoms towards the science chamber, as seen in Fig. 5. It has been experimentally set as $10:1$. In the final destination, five beams and another set of magnets create a 3D MOT. Five beam configurations come from using 4 independent horizontal beams and one retro-reflected vertical beam. The final trap is at a distance $d = 61(6)$ cm from the first. The 2D MOT is set above the 3D MOT $\Delta z = 3.0$ mm. This compensates the sink in the z-axis due to the gravitational force. The atomic beam arrives at the science chamber at an angle of 25° to the closest horizontal laser beam. The group achieved a peak flux, coming from 2D MOT, of $4 \cdot 10^8$ atom/s for parameters shown in Tab 10. The measured trapping rate was around $3.5 \cdot 10^8$ atom/s.

5.1.2 Original simulation

In the article this optical system has been modelled using a numeric Monte Carlo simulation, where it was assumed that the 2D MOT was loaded from the background Cs vapour. The initial velocity distribution of the atoms was assumed as a Maxwell-Boltzmann distribution (at temperature $T = 300$ K). To initiate an atom its velocity was picked from this distribution and its position was randomly set in the glass cell. Forces have been established according to the theory presented in 1. The Doppler forces from each laser beam were summed and then the classical Monte Carlo trajectory simulation was performed. In the process, simulation determines if an atom is captured in the 2DMOT, then if it reaches the 3DMOT region in the science chamber, and finally if it is captured by the 3D MOT. The simulation ends each trajectory if the atom hits a wall. After running 300,000 trajectories, the capture efficiency α is calculated. It is the number of atoms trapped in the final trap divided by the number of simulated objects. The loading rate was estimated by

$$L = \alpha \frac{N_{\text{cell}}}{\tau_{\text{capture}}}. \tag{5.2}$$

The number of Cs atoms in the cell N_{cell} was determined by an experimental time-of-flight measurement. The 2D MOT loading time $\tau_{\text{capture}} = 11.5$ ms was a constant determined in the model. It is the average time it takes for an atom to be captured in the 2D MOT. The loading rate was estimated as $L = 5(4) \cdot 10^7$ atoms/s. This model provides only the capture efficiency of the system and, to obtain the trapping rate, it is crucial to build and measure the experimental setup. The simulated trapping rate was of an order smaller than the measured value, which was attributed to the underestimation of the capture efficiency, by the model. It assumed that atoms hit the glass cell wall and stick to it. In the experiment there has been no metal build up observed on the walls, which meant that atoms desorbed and re-joined the cooling dynamics

5.1.3 Our simulation

Now we will present how this experimental set-up was analysed by our program. The program was set to save subsequent positions and velocities for each atom every 100th iteration. Each step is $\Delta t = 1$ μs and the whole simulation time was $t = 0.1$ s. We chose step size $\Delta t = 1$ μs as optimal. Choosing a step size that was too large would have reduced the precision of the simulation and could have caused some elements of the evolution to be missed. Choosing a step size that was too small would have meant significantly longer calculations, especially since we assumed the time of the entire simulation to be $t = 0.1$ s. Laser cooling calculations have been set to address 852 D2 transition with the mass of the particles $m = 133$ u. Gravitational force has been initiated. Since the atoms are captured from a background gas we have created six rectangular effusion surfaces at the limits of cooling volume, which is the overlap of all the beams in the 2D MOT. Surfaces created a rectangular box $2R_{\text{2D}}$ x $2r_{\text{2D}}$ x $2r_{\text{2D}}$, where r_{2D} is the minor radius and r_{3D} is the major radius of the 2D MOT laser beam. This approach was done according to the theoretical model of [21].

Each of the effusion surfaces emitted atoms in the inner direction. The number of atoms to be emitted per surface was set by the number of all atoms scaled by the ratio of the single surface to the sum of all surfaces. In AtomECS they are described as 3D objects so their thickness was set as 1 mm. Four laser beams have been added with an as-provided (Tab. 10) detuning, intensity, radius, and ellipticity. Their smallest waist has been set at the $(0, 0, 3.0)$ mm point. The beam diverges according to its Rayleigh waist. Lasers' direction was set to be perpendicular to each other, in the YZ plane and at an angle of 45° to a Y axis. Their polarisation was set to be circular. Both were set to be the same handedness since polarisation for a laser object is set according to the direction of the local magnetic field. In the AtomECS world beams perpetuate in infinity so we could not add a counter-push beam since it would disturb atoms in the 3D MOT. To preserve its influence the push power has been decreased by 25%. This number was calculated by comparing forces exerted on an atom in an asymmetric 1D optical

molasses, and a single push beam. We have not included the repump beams and have not initiated the possibility for the atom to fall into a dark state. By doing so we presume that the repumping efficiency is 100%.

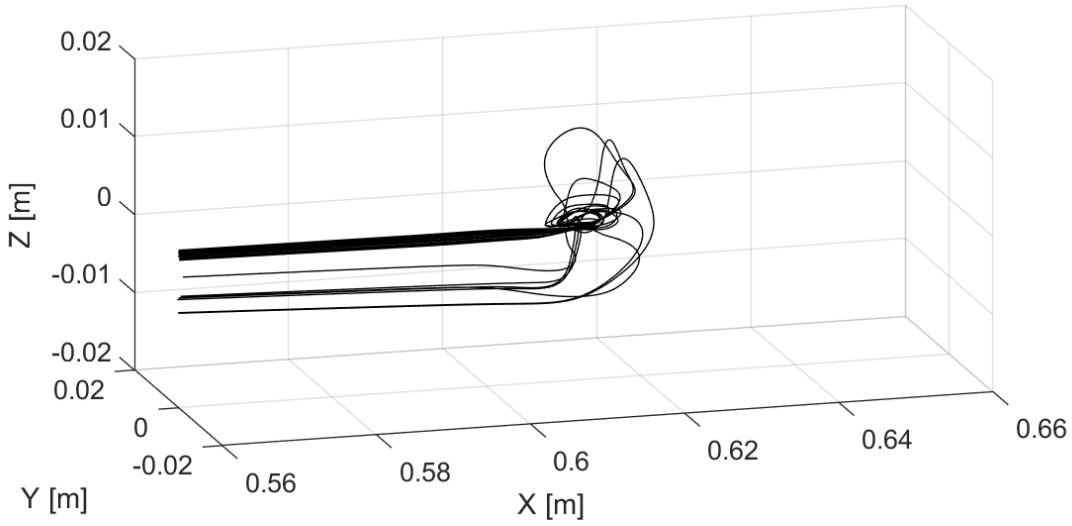

Figure 6: Trajectories of atoms in three axes in the vicinity of the 3D MOT. Only atoms that have been trapped are shown. The plot shows volume around the position $x = 0.61$ m.

Quadrupole magnetic gradient has been added with a symmetry axis set as X. Magnetic field covers the same centre as laser beams. The 3D trap has been constructed similarly, adding a pair of lasers to trap in all three axes. The power is split accordingly: 10 mW for 4 horizontal beams and 20 mW for a retro-reflected vertical beam, which creates a stronger cooling in the Z axis. The magnetic field symmetry axis coincided with Z. Distance between intersections of lasers in 2D MOT and 3D MOT was set as $d = 610$ mm. We have added bounds to the simulation. They were: a box of glass cell's dimensions, a narrow 1.5 mm wide tube, a wider tube for the atomic beam to propagate, and the space chamber. The last two boundaries are big enough to limit solely the outliers' movements. Lastly, a velocity cap was set as $v_{\max} = 70$ m/s.

Table 11: Simulation estimations of capture velocity v_c, trapping efficiency α, and trapping rate L provided in the article [22] and calculated with our program.

	Original simulation	Our simulation
v_c [m/s]	20.6 ± 1.0	22.5
α	$6 \cdot 10^{-5}$	$9 \cdot 10^{-5}$
L [atoms/s]	$5(4) \cdot 10^7$	$(6.18 \pm 0.05) \cdot 10^6$

The originally measured trapping rate, as seen on Tab. 11, was an order smaller than the experimentally measured by the group $L = 3.5 \cdot 10^8$. This difference was justified by the underestimation of the capture efficiency by the original model. It assumed that atoms hitting the glass cell wall stick to it. The group did not

observe any metal build-up on the glass cell, which signified that atoms could desorb and re-enter the cooling dynamics. This assumption is also reflected in our simulations.

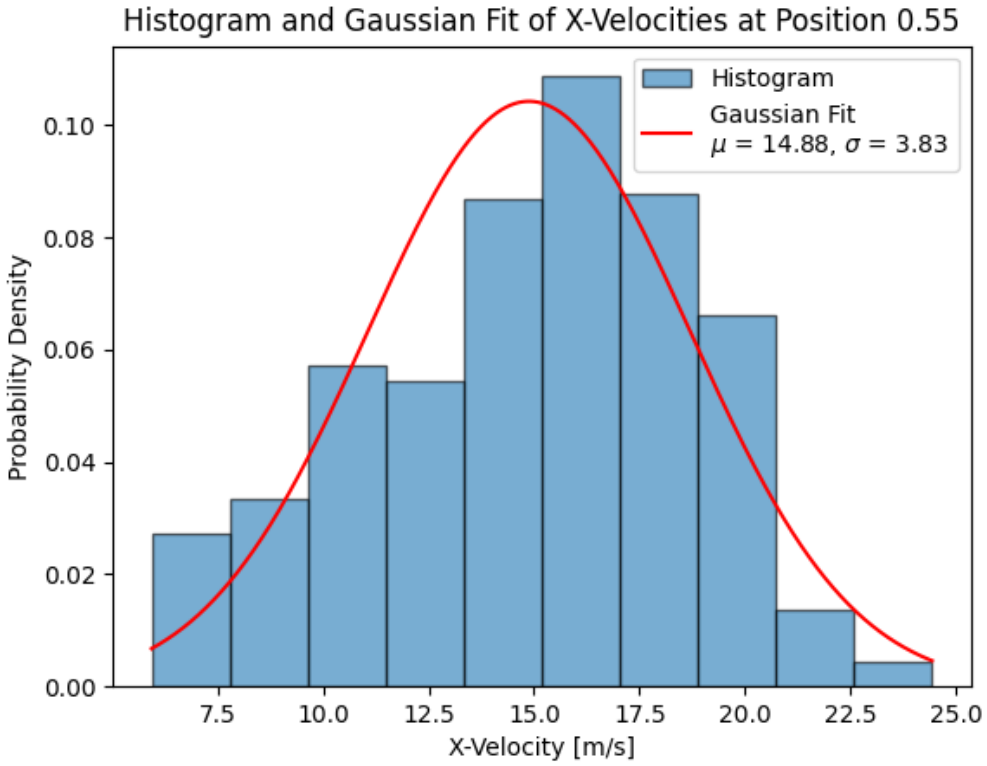

Figure 7: Velocity distribution of atom just before the 3D MOT with a Gaussian fitting. Number of analysed atoms was 575.

Our simulation provided efficiency in the same order. Comparing the provided trapping rates we see that our result is of an order smaller, but after performing a Z-test we can state that those variables are separated by a 1.1 standard deviation from each other making them not statistically different. This is largely due to the big uncertainty of the original approximation. Moreover, we have analysed the velocity distribution of an atomic beam coming from the 2D MOT. In an experimental setup, this is done by acquiring fluorescence in the science chamber (without the 3D MOT beams present) while at the same time, the 2D MOT is abruptly shut down. The signal decreases approximately in the shape of an error function. By integrating it we get a Gaussian distribution of velocity. It's important to mention that it measures the mean velocity of the atom not the actual velocity in the plane of the measurement. To replicate it in the simulation, we calculated the time it takes for every atom to arrive at a plane just before the 3D MOT (since the forces of the 3D MOT are still present). Capture velocity is shown in Tab. 11 and the parameters of the distribution in Fig. 7. We have defined capture velocity as two standard deviations above the mean. For context, the measured capture velocity was $v_{mc} = 26(1)$ m/s. Our simulation predicts the main characteristics of the system well compared with an established simulation. It correctly estimates not only values like efficiency or capture velocity but also

trapping rate which originally was calculated using a measured variable, validating our model of the atomic source.

5.2 Potassium

A second simulation, of the first realised bright source of cold potassium atoms, was performed. It was used to create K-Rb molecules, a Bose-Bose mixture [21] [60]. We have simulated a 2D+ MOT for ^{39}K. We underline that we neglect the hyperfine structure in the simulation which can be especially important in the case of potassium as explained in section 4.1.2.

5.2.1 Experimental setup

As in the previous setup properties of potassium allow for loading the 2D MOT directly from the background gas. To sustain the vapour pressure a set of dispensers is used. Potassium has three stable isotopes and they are released in a natural abundance mixture, from the dispensers. The chamber containing the source is connected with the ultra-high vacuum (UHV) science chamber by a 10 cm bellow. The output of the 2D MOT chamber was a 1 mm wide hole drilled inside a 45° mirror. As before, a mirror was used to introduce push and counter-push beams. A hole in the mirror allowed for the transfer of atoms. It also maintained a differential pumping of 10^{-4} pressure ratio.

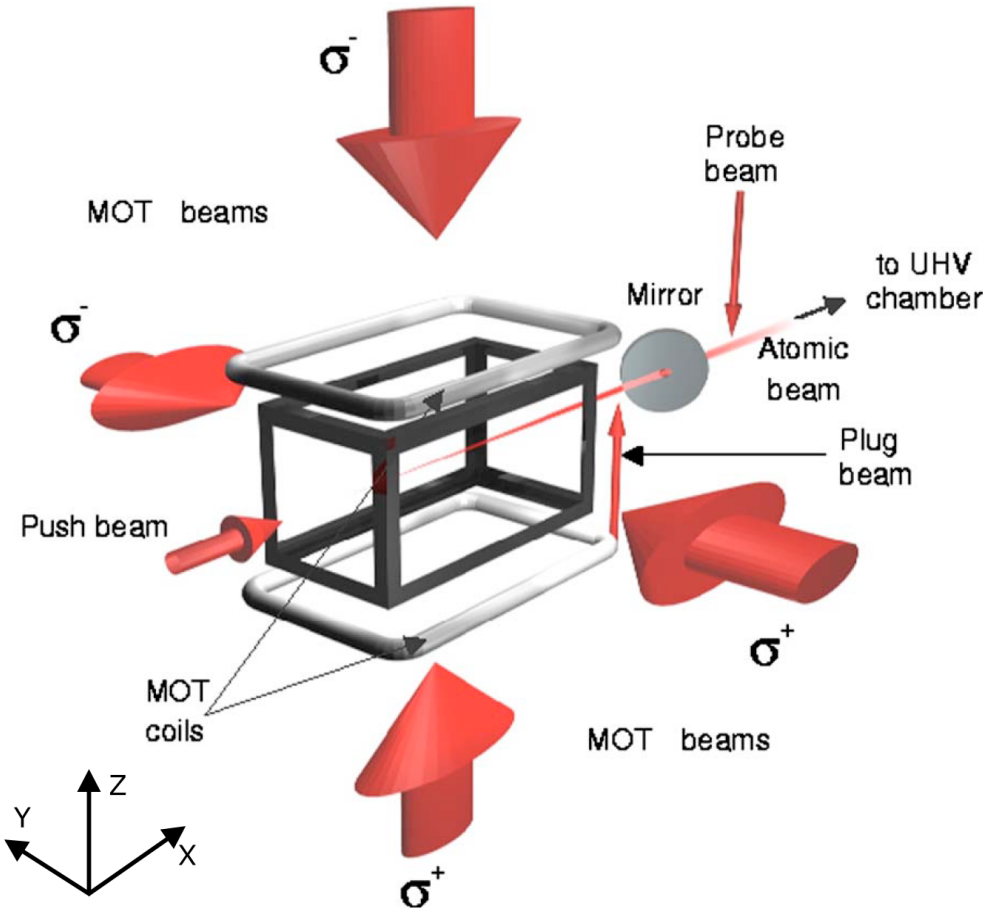

Figure 8: Scheme of the Jacopo Catani's experimental setup. Accommodated from [21] with a modified coordinate system to match the one of simulation.

The quadrupole magnetic field is generated by a pair of rectangular coils, fixed around glass windows. Due to the chamber's geometry, the coils were elongated in the X axis but it still gave the required, almost 2D axial, symmetry to the trapping field. The magnetic gradient in the y-z plane is set to 17 G/cm. The current in the coils was adjusted to compensate for stray magnetic field due to which the longitudinal magnetic gradient along x is a factor of 10 smaller than in the y-z plane.

Table 12: Characteristics crucial for the simulation of the documented experimental setup of a 2D+ MOT for potassium atoms. We include wavelength λ, radius R, power P and detuning δ for lasers that create the trap and the push beam (denoted by '+'), the gradient of used magnetic field ΔB.

Parameters	Value
λ [nm]	767.5
R_{2D} [mm]	14.1x4.7
R_+ [mm]	0.75
P_{2D} [mW]	80
P_+ [mW]	6
δ_{2D} [Γ]	-5.8
δ_+ [Γ]	-5.2
∇B_{2D} [G/cm]	17

The laser light used for cooling had a wavelength of 767.5 nm. The cooling beams had a 3:1 elliptical shape, with a smaller waist of 9.4 mm. Two such beams were circularly polarised and retroreflected creating a 2D-MOT. The maximum laser power was 80 mW. Along the z-axis direction, an additional σ_+ polarized beam was inserted. It was called a push, with a waist of 1.5 mm. A counter-push beam was also introduced using the 45° mirror. It had a hollow profile since it entered the 2D-MOT after reflection upon the drilled mirror. Another vertical beam called a plug was used to perform the time-of-flight (TOF) measurements after the 2D+ MOT.

5.2.2 Performed simulation

The numerical simulation done in the discussed experiment was based on the numerical integration of the equations of motion which gave a phase-space trajectory. The simulation begins with atoms at the 2D MOT boundary, a rectangular box with dimensions of the lasers' waists. From the integration, the fraction α was extracted. It was defined as the ratio of the atoms exiting the mirror hole to the atoms entering the 2D-MOT volume. To obtain the total flux, the total number of atoms entering the cooling volume per second, at pressure p and room temperature T was multiplied by α:

$$\Phi = \alpha S \frac{p}{\sqrt{2\pi m k_B T}}. \tag{5.3}$$

Variable S is the surface emitting atoms. From the simulation, the longitudinal velocity distribution of the atomic beam, and the distribution of the cooling time can be obtained. The simulation neglected multiple scattering of light and intra-beam atomic collisions. The collisions with background gas were accounted for by weighting each trajectory with a factor $\exp(-\gamma t_c)$, where the collision rate was set as $\gamma = 60\ \mathrm{s}^{-1}$. Moreover, the model deleted atoms that were flying in a cone 34 mrad wide around the longitudinal axis X. Setting the experimental parameters

as in Tab. 12, the group obtained total flux as $\Phi_{\text{sim}} = 8.7 \cdot 10^{10}$ atoms/s, where the measured flux was $\Phi = 6.2 \cdot 10^{10}$ atoms/s.

5.2.3 Our simulation

In this section we present simulation of the aforementioned only a 2D MOT with a push beam so only those objects were put inside the world. We did not initiate gravitational force since the article did mention gravitational acceleration in the simulation.

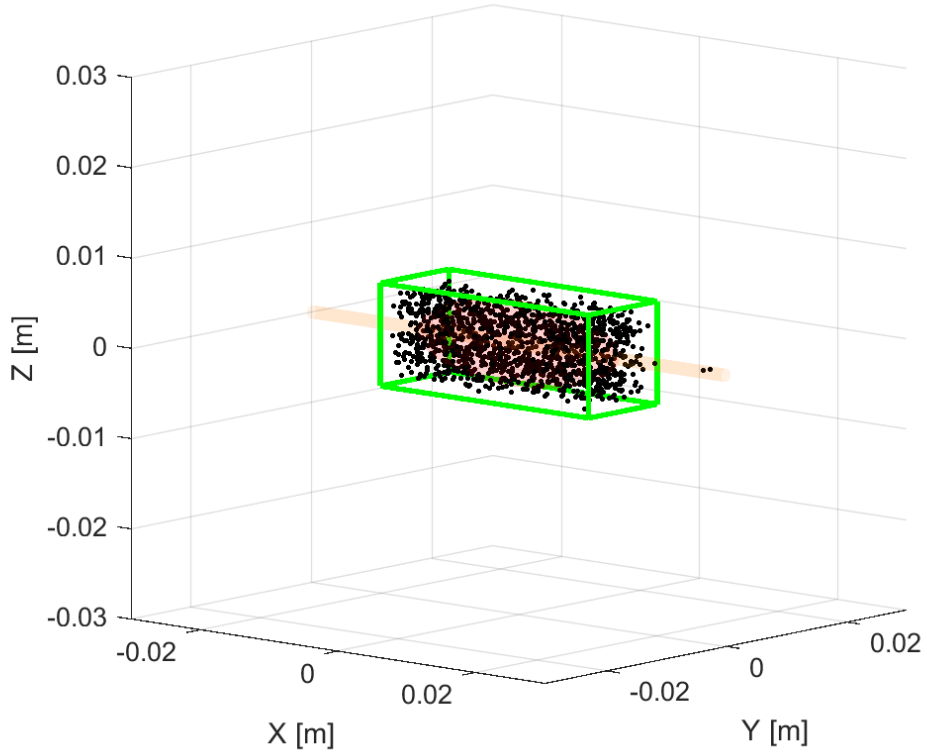

Figure 9: Visualisation of a 2D MOT for potassium atoms. Where the green lines depict the borders of effusing surfaces, the red ellipsoid - cooling volume and the orange tube - push beam.

Parameters were set as in Tab. 12 for solely the cooling laser beam at wavelength $\omega_1 = 767.5$ nm. We are not able to simulate interaction with two transitions and also the parameters for repump were not specified. Contrary to the previous simulation we have not scaled down the power of the push beam to take into account the influence of the counter-push beam since the ratio between them was not specified.

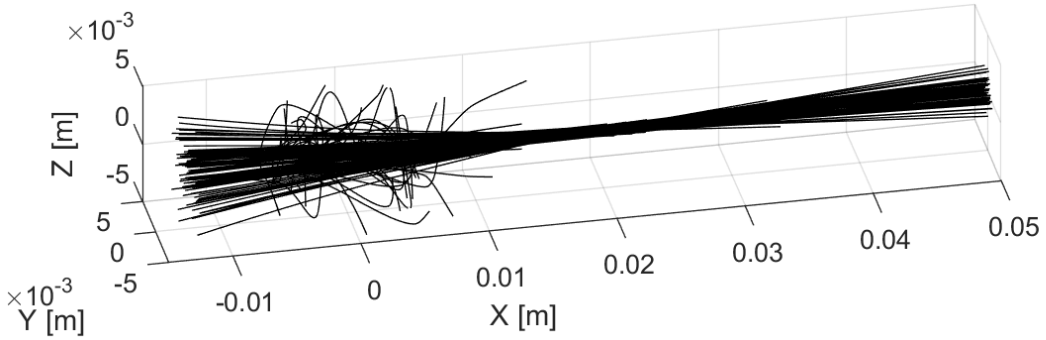

Figure 10: Trajectories of atoms in three axes. Only atoms that have been trapped are shown. The plot shows volume around the 2D MOT and after the differential pumping tube.

The magnetic field was set of axial symmetry and of gradient $\nabla B = 17$ G/cm in the YZ axis.

Table 13: Simulation estimations of trapping rate L provided in the article [21] and calculated with our program.

	Original simulation	Our simulation
L [atoms/s]	$8.7 \cdot 10^{10}$	$(2.56 \pm 0.54) \cdot 10^{9}$

Limiting space for the chamber and the tube after the small pipe was set to be big enough to only delete outliers. Beside a 1 mm pipe we have added a thin tube of radius 1.2 mm at a distance 35 mm to filter out atoms diverging at an angle bigger than 34 mrad. The calculated flux was significantly lower than the one of the original experiment. This could be due to the lack of a repumping beam which in the case of potassium is an integral part of the cooling scheme. Additionally, the source of the discrepancy could be the desorption of atoms from the wall of the chamber, as it was the case for caesium.

5.3 Silver

The last proof-of-concept simulation was of silver atoms trapping and cooling system realised by the group [25] [61]. It is the only MOT for this element and to our knowledge, there are no performed simulations of silver atoms in a magneto-optical trap. We have simulated a 3D MOT loaded with ^{109}Ag directly by an oven.

5.3.1 Experimental setup

Laser setup consisted of 40 mW laser beam at 328 nm. It was superimposed with the repumping light which had a few milliwatts of power. It was divided into

three parts to form the trapping beams of the MOT, which were retro-reflected in 3 axes.

Table 14: Characteristics crucial for the simulation of the documented experimental setup of a 3D MOT for silver atoms. We include wavelength λ, radius R, power P and detuning δ for lasers that create the trap, the gradient of used magnetic field ΔB, and the distance d between the atomic source and the trap.

Parameters	Value
d [mm]	500
λ [nm]	328
R_{3D} [mm]	3
P_{3D} [mW]	1.5
δ [Γ]	-1.0
∇B_{3D} [G/cm]	10

The vacuum system consisted of two chambers. The first one contained an oven in the form of a ceramic crucible heated by a tantalum wire to produce an effusive atomic beam. It was operated at 1200 K. The background pressure was measured to be $2 \cdot 10^{-9}$ mbar. The beam was collimated by two apertures after which it entered the second chamber through an opening 1 mm wide to guarantee differential pumping. The distance between the oven and the trap centre is 0.5 m, denoted as d. Because of the low laser power available and the complexity of the laser system, it was decided to load the trap directly from the thermal atomic beam without any further beam slowing. In addition, a second oven located 3 cm from the centre of the trapping region was inserted to be used as an additional source. It was a small filament of thin rhenium wire to which a small droplet of molten silver was applied. It worked as a dispenser. In the article the trapping rate was not directly mentioned but we have calculated it knowing that the number of trapped atoms was 10^6 and the trap's lifetime was said to be $\tau = 16$ s, which gives a trapping rate of $L = 6.3 \cdot 10^4$ atoms/s.

5.3.2 Our simulation

Even though the experiment did not cover any simulation of the setup we still wanted to perform one to verify how our theoretical predictions match the experimental result, before proceeding to simulations of the new system, currently under construction in our laboratory.

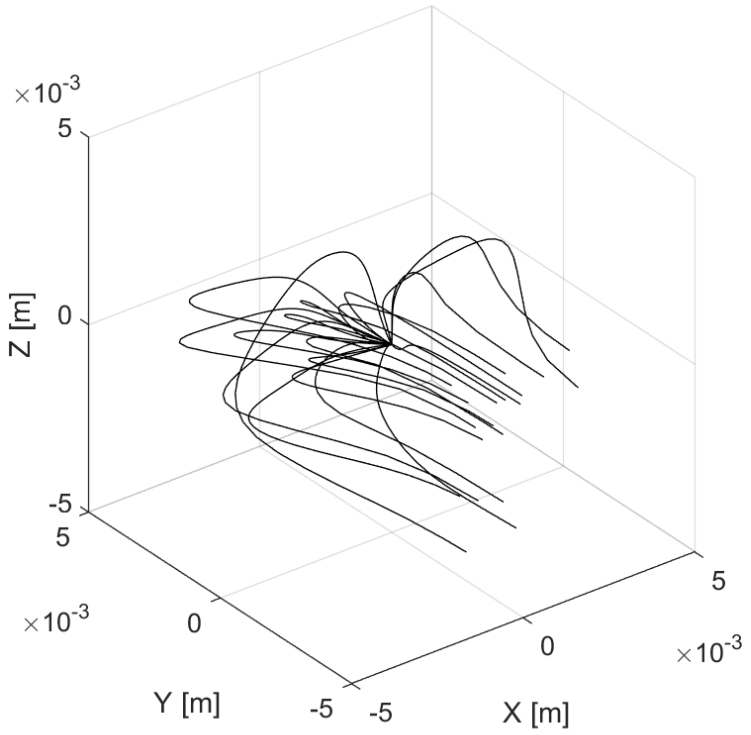

Figure 11: Trajectories of atoms in three axes in the vicinity of the 3D MOT. Only atoms that have been trapped are shown.

Specific elements of this system were the use of an effusion cell instead of the background gas, and the very low efficiency of the trap which requires simulating a large number of objects. The gravitational field was initiated since the distance between the cell and the trap was substantial and we wanted to recreate the specifics of the trap as closely as possible. The 3D MOT was constructed as for the previous setup, with 6 beams and a magnetic quadrupole field with Z-axis symmetry.

Table 15: Simulation estimations of trapping rate L provided in the article [25] and calculated with our program.

	Original measurement	Our simulation
L [atoms/s]	$6.3 \cdot 10^4$	$1.1 \cdot 10^5$

Individual parameters were set as in Tab. 14. Since the efficiency of the trap is low and the temperature of the effusion cell is very high with no other slowing mechanism atoms with velocities below capture velocity are scarce. To simulate the trap going around this issue we have sampled the atom's velocity for Maxwell-Boltzmann distribution at room temperature $T = 300$ K and then scaled the obtained flux with a ratio

$$\eta = \frac{\int_0^{40} f(v, m_{\mathrm{Ag}}, T = 1200\ \mathrm{K})dv}{\int_0^{40} f(v, m_{\mathrm{Ag}}, T = 900\ \mathrm{K})dv} \approx 0.127, \tag{5.4}$$

where $f(v, m, T)$ is the Maxwell-Boltzmann velocity distribution. The cell's pupil was simulated as a 1.1 x 1.1 mm square, 1 mm thick. After the effusive output, we inserted a tube 20 mm wide and 495 mm long, where atoms could freely propagate. Before the science chamber, an aperture was put in, that filtered all the atoms that wouldn't interact with the lasers. It was 6.8 mm wide and 0.5 mm long. Lastly, the space for the 3D MOT was added as a 9 x 9 x 9 mm cube. The velocity cap was set to 40 m/s so that we wouldn't simulate atoms with much higher initial velocity than the capture velocity.

When calculating the initial flux coming from the hot source we used the model explained in 2.3 for a non-ideal effusion cell. We assume that the dimensions of the body of the cell are ideal but the orifice and the evaporation coefficient are not. We have calculated the correction factor as $F_N = 0.27$ [39]. As seen in Tab. 15 we have obtained the trapping rate almost twice bigger than it was measured. This discrepancy could be because the rate was calculated using measured parameters that are established with little accuracy. For previous simulation estimated trapping rate was an order smaller than the measured value which we explained partly through desorption of atoms from the chamber's walls. In the case of silver we don't see this decrease, because the walls are at room temperature at which silver has very low evaporation rate.

5.4 Conclusion

We have performed three simulations representing different experiments. They differed with the laser beam parameters, magnetic field, atomic species, layout and the types of traps used. Our simulation provided an estimation close to the one simulated or measured. This showed that the simulation based on AtomECS software with additional modelling of the atomic source is a robust, versatile and sufficiently accurate tool.

6 Novel configuration for ultracold molecules

Historically, each research group developed their own simulations to predict the performance of the cooling process in each constructed experimental setup [21, 22]. Optimization was usually based on the experience of the group members and was rarely a streamlined process [28]. Often, simulations required some experimental input such as the velocity distribution of atoms in the beam emitted by the 2D MOT [22, 28]. As a result, simulations were mainly tools to show that the cooling process in a given experimental setup was well understood, but rarely provided predictive power useful for the actual optimization of the parameters at the design stage. However, the underlying physics was always the same, and over time several

software packages that allow simulation of the cooling process were developed. We decided against writing the entire simulation from scratch and opted for adapting existing software to meet our needs. In this way, we increased the probability that the chosen approach will be robust, easy to use and explain, and give sufficiently reproducible results while allowing a quick optimization useful for designing a new setup. This chapter presents results of simulations that predict the performance of the setup that is currently being constructed in our laboratory.

6.1 An overview of the constructed experimental setup

We have devoted this chapter to describing a novel experimental setup for creating KAg and CsAg molecules. Based on the constraints imposed by the design choices, we identified the relevant parameters for the simulation and derived their optimized values. The beam radius, ellipticity, and shift in the z-axis have been defined as in Section 5.1.1. The size of the orifice of the effusion cell is described by b_x and b_y. We have introduced the total available power of laser beams P_{total} and the ratio $\zeta = P_{\text{2D}}/P_{\text{total}}$, which characterizes how much of total available power is directed to the 2D MOT. This will allow us to optimize the power of each beam and, at the same time, the total power used for the system.

6.1.1 Vacuum system

The vacuum system shown in Fig. 12 comprises three main sections. The 2D MOT chamber for silver is based on a 6-way stainless steel cross that has four 7.6 cm diameter windows for laser cooling beams. The windows are relatively large, so they do not restrict the size of the cooling beam. The dimensions of the cross restrict the possible location and size of the source of silver atoms, but the chosen design is useful to minimize the possibility of coating the windows with the beam of atomic silver. The source of silver, a crucible filled with silver pellets, should be located as close to the 2D MOT axis as possible to guarantee a high flux of emitted atoms even when operated at a (relatively) low temperature (which would still be on the order of 900 °C). Due to restrictions imposed by the geometry of the cooling beams, the source cannot be closer to the 2D MOT axis than approximately $\sqrt{2}\times$(cooling beam radius). It also places constraints on the size of its orifice in the plane of the beams. The size of the pupil in the y direction,b_y, can only be twice the distance from the beam overlap. Taking into account the dimensions of the chamber and the possible size of the beam, we have established the limit at 25 mm. We set the same limit for the size of the orifice in y-axis b_x. It is not constrained but we do not expect it to be larger than the width of the beam in the major axis of the ellipse. This chamber is pumped with an ion pump to ensure ultra-high vacuum conditions and is separated from the main chamber with a gate valve. An additional window on the very left of the chamber is used to insert the push beam for the silver 2D MOT.

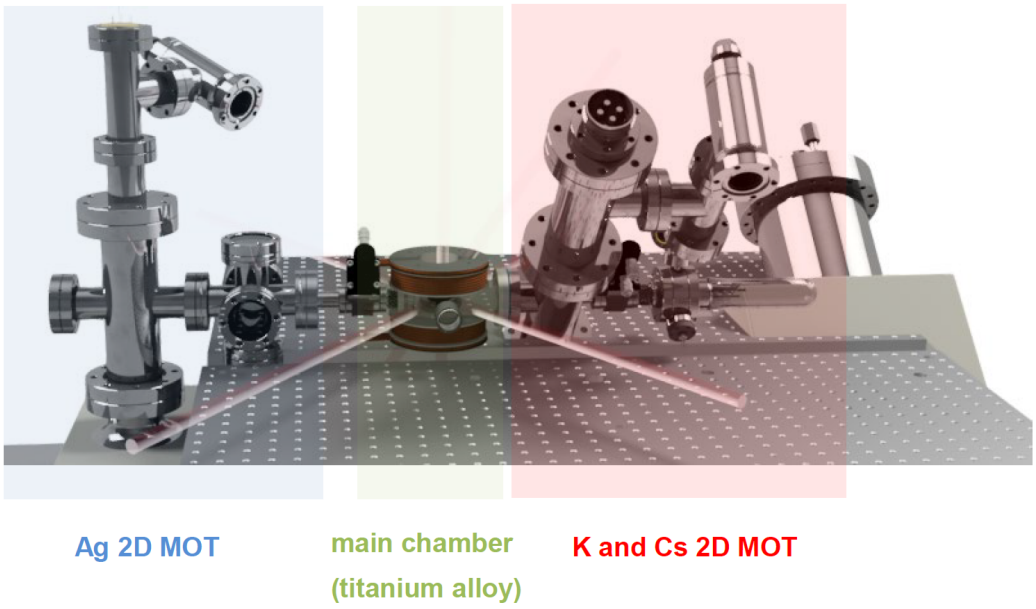

Figure 12: Rendering of the vacuum system of the constructed setup. Courtesy of dr Mariusz Semczuk.

The custom-made titanium alloy main chamber, where the actual experiments will take place, was intentionally designed to be small to ensure that the magnetic coils could be placed as close to each other as possible, here at 30 mm separation. This reduces the requirements for the current required to generate the magnetic fields needed for the experiment. As a result of this design choice, the diameter of the cooling beams for the 3D MOT cannot exceed 20 mm. The location of the trapped atoms is 21 cm away from the silver 2D MOT and 35 cm from the K/Cs 2D MOT.

Finally, the third chamber on the right is based on a glass cell and houses a dual-species (K+Cs) 2D MOT. With the glass cell, magnetic coils can be positioned closer to its symmetry axis, making it easier to achieve high magnetic field gradients. The glass cell can be used for alkali atoms because they are easily evaporated, and if stuck to the glass surface, they can be desorbed with UV-LED light. Here, atoms are loaded directly from the background gas.

All chambers are separated with differential pumping tubes to ensure that a pressure on the order of 10^{-11} mbar can be reached in the main chamber.

6.1.2 Laser systems

We have established the geometrical constraints of the system. We need to now establish the limits for parameters of the cooling lasers and the magnetic field. For caesium and potassium, existing laser systems will be used [62, 63]. The laser system for silver, briefly discussed below, is more of an unknown because it is currently under construction and we can only estimate what powers will be available. The first constraint we put on the 3D MOT is the same beam size for each species,

but this is mainly for convenience - in the actual experiment it makes it a little easier to align the beams if they are roughly the same size. Another one is that the magnetic field of the 3D MOT has to be the same for trapping all considered species because silver and one of the alkali species will be trapped simultaneously in the 3D MOT. It is a fairly established approach in many experiments with ultracold mixtures. Based on these considerations, we identified the boundaries (see Tab. 16) for the experimental parameters that will be optimized in this work.

Table 16: Limits set for the parameters before optimising them.

Parameters	Notation	Ag	K & Cs
Total power	P_{total} [mW]	300	300
Ratio $P_{\text{2D}}/P_{\text{total}}$	ζ	$[0.6, 1.0]$	$[0.1, 1.0]$
Ellipticity	ϵ	$[0.5, 1.0]$	$[0.5, 1.0]$
Detuning	δ [Γ]	$[-5.2, -2.2]$	$[-6, -3]$
Push beam power	P_+ [mW]	$[0, 2]$	$[0, 2]$
Push beam radius	R_+ [mm]	$[12, 18]$	$[12, 18]$
2D MOT beam radius	R_{2D} [mm]	$[12, 18]$	$[12, 18]$
Shift in z-axis between traps	Δz [mm]	$[0, 5]$	$[0, 5]$
Pupil size in x-axis	b_x [mm]	$[0.5, 25.0]$	—
Pupil size in y-axis	b_y [mm]	$[0.5, 25.0]$	—
Magnetic gradient of 2D MOT	ΔB_{2D} [G/cm]	$[10.0, 60.0]$	$[1.0, 20.0]$
Magnetic gradient of 3D MOT	ΔB_{3D} [G/cm]	$[1.0, 20.0]$	8.5

For laser cooling of silver, a laser source at 328 nm is needed. Direct sources are not available at this wavelength. The approach we have chosen relies on two high-power fiber amplifiers emitting at 1120 nm and 1584 nm. These beams are then combined in a non-linear crystal to generate 5 W of 656 nm light via sum frequency generation. Finally, a second-harmonic generation cavity is used to convert the 656 nm light into 328 nm light. The expected output in UV should be around 1 W. In order to ensure that the radiation is precisely at the desired frequency, we will implement frequency stabilization methods. The frequency of the light provided by fiber amplifiers is very stable, therefore we assume that initially we will monitor the 656 nm light with a wavemeter and use it to correct the frequency of the 1120 nm laser to make sure that the frequency of the 328 nm does not change. To improve frequency stability, we plan to use molecular iodine, which has a transition at a frequency $\approx$ 600 MHz away from the required frequency of the 656 nm light. The spectroscopic signal will be used to correct the frequency of the 1120 nm laser. Both of these approaches rely on the good passive frequency stability of the 1584 nm laser.

Ultimately, the 328 nm light will be frequency-stabilized using an optical frequency comb. A beatnote between the comb and the 1120 nm as well as the 1584 nm laser will be stabilized, therefore providing absolute frequency determination in the UV. This relies on the fact that we can represent the frequency of each fundamental laser by comparing it to a frequency comb with the repetition

frequency f_{rep} and the carrier envelope offset frequency f_{CEO} as:

$$\begin{aligned} f_1 &= n_1 f_{\text{rep}} + f_{\text{CEO}} + f_{\text{beat},1} \\ f_2 &= n_2 f_{\text{rep}} + f_{\text{CEO}} + f_{\text{beat},2}, \end{aligned} \tag{6.1}$$

where indices 1 and 2 refer the 1120 nm and 1584 nm lasers, respectively. Here, n_i is the number of tooth to which the lasers are locked and $f_{\text{beat,i}}$ is the beatnote between the laser and the comb tooth n_i. The frequency f_3 of the 656 nm light can be expressed as:

$$\begin{aligned} f_3 = f_1 + f_2 &= n_1 f_{\text{rep}} + f_{\text{CEO}} + f_{\text{beat},1} + n_2 f_{\text{rep}} + f_{\text{CEO}} + f_{\text{beat},2} \\ &= n f_{\text{rep}} + 2 f_{\text{CEO}} + (f_{\text{beat},1} + f_{\text{beat},2}), \end{aligned} \tag{6.2}$$

where $n = n_1 + n_2$. It is now sufficient to determine n based only on the readout of the frequency f_3^{WM} of the 656 nm source with a wavemeter:

$$[n_2] = \frac{f_3^{\text{WM}} - 2 f_{\text{CEO}} - (f_{\text{beat},1} + f_{\text{beat},2})}{f_{\text{rep}}}. \tag{6.3}$$

Due to the presence of hyperfine splitting in the ground state of silver, to have control over the laser cooling process, we need to derive both the cooling and the repumping beams from the stabilized laser source. For this purpose, we will use an electro-optic modulator (EOM) such that the carrier will be the cooling beam ($\approx 40\%$ of power) and the +1 sideband ($\approx 30\%$ of power) will be the repumping beam. The -1 sideband will be sufficiently far detuned from any transitions to not cause any issues during the cooling process. Additional frequency shifts will be introduced by acousto-optic modulators (AOM) in a double-pass configuration. These will be needed to provide frequency tuning capability. They will also act as both fast shutters and laser power regulators. For an optimized AOM, the typical diffraction efficiency is $\approx 80\%$, with $\approx 60\%$ total efficiency expected in a double-pass configuration. Ultimately, neglecting all other losses, we would expect at most 450 mW of total UV power to be available for the experiment. As these are only provisional estimations, for the purpose of the simulation we decided to assume that the total power would not exceed 300 mW.

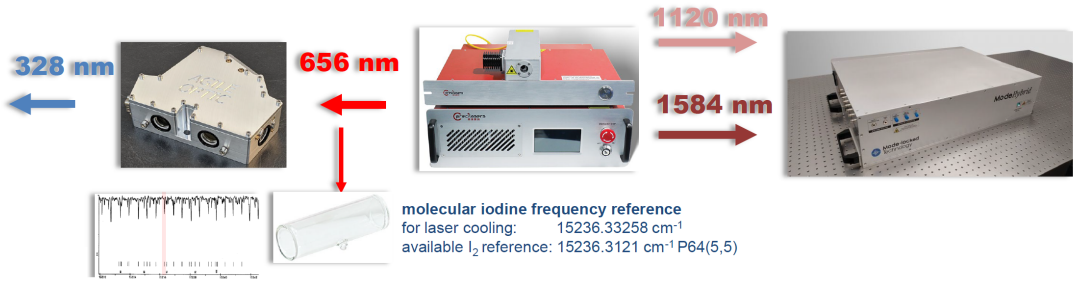

Figure 13: Scheme of the laser system. Courtesy of dr Mariusz Semczuk.

6.2 Results of the simulations of the designed system

With the provided scheme and the established limits, we have written 3 simulation scripts for every atomic species. The general layout was presented in the previous

chapter. We used them to optimize the system parameters by Bayesian optimization. With the new values, we have simulated the trajectories and characterized the setup. The caesium script has been presented in Section 4.3 as an example of our simulation. Because potassium has similar physical properties to caesium and the 2D MOT is also loaded from the background gas at room temperature, its segment ultimately has the same simulation layout, but with different values of the parameters specific to a given atom. Due to the fact that there are up to twelve changeable variables, we decided to optimize four at a time, which allowed more control over the process. The exemplary calculation shown in Fig. 4 took seven hours and returned optimized values for the radius and the power of the push beam, the ellipticity of the cooling beams, and the shift in the Z axis.

Table 17: Final values of optimised parameters for every part of the system.

Parameters	Cs	K	Ag
P_{sum} [mW]	300	300	300
ζ	0.65	0.51	0.83
ϵ	0.84	0.94	0.56
δ [Γ]	-4.86	-5.48	-2.72
P_+ [mW]	0.89	0.51	0.49
R_+ [mm]	1.4	1.95	1.62
R_{2D} [mm]	5.5x3.0	18.4x6.3	12.4x10.3
R_{3D} [mm]	7.5	7.5	7.5
Δz [mm]	1.5	1.5	2.0
ΔB_{2D} [G/cm]	8.34	3.94	12.89
ΔB_{3D} [G/cm]	8.5	8.5	8.5

The silver segment was simulated with an analogous script. Since the atomic source is an effusion cell, only one oven entity was created and placed directly below the crossed beams. This differs from the previously discussed design, where the crucible was on the side of a beam parallel to the Z axis. Nevertheless, it is essentially the same, since the atom's velocity is much higher than the differences acquired from the gravitational force. In the simulation, we set the distance between the oven and the MOT to be 15 mm. Such a number was set by assuming $R_{\text{2D}} = 8$ mm and $\epsilon = 0.67$ (initial values before optimisation) and adding additional safe space. The closer to the trap we will place the higher the flux. After optimisation, the minimal value for this distance is 14.54 mm which means that the crucible will have to be moved further away to fit not only its orifice but also its body. The size of the crucible's pupil was additionally optimised and we allowed for an elongated shape. An elongated oven output would resemble the shape of the cooling volume increasing the flux from the 2D MOT. In the simulation, we have also added a `SimulationVolume` that will hold the oven and the space leading to the trap. When considering the layout for silver we performed a simulation where we simply inserted the crucible close to the 3D MOT. It didn't yield better results.

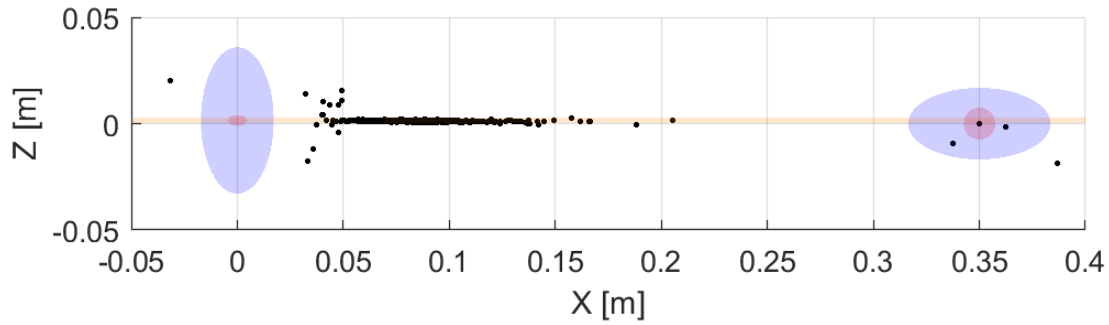

(a) .

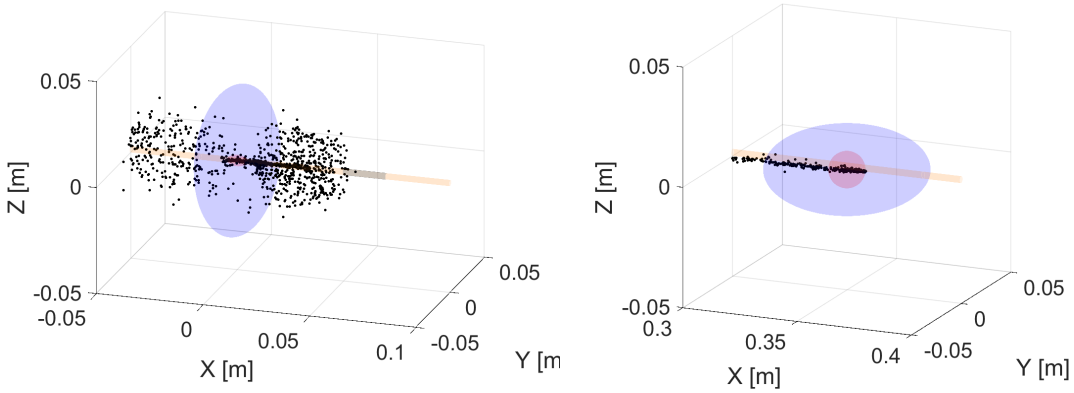

(b) (c)

Figure 14: Visualisation of atoms in the cooling system for caesium. The blue ellipsoid represents where the Zeeman shift is equal to the detuning of the laser, the red ellipsoid shows the laser cooling volume with the $1/e^2$ radius, the orange shows the push beam and the grey, the differential pumping tube. The system is shown from three perspectives: a) full view, b) 2D MOT close-up, c) 3D MOT close-up.

We simulated and characterised each part of the system for the new parameters noted in Tab. 17. Velocity distribution at a position before the 3D MOT is presented in Fig. 15. It includes only the atoms caught by the 3D MOT. They have consistently a Gaussian distribution. From the fitted Gaussian function we have obtained the mean velocity μ and the standard deviation σ. It was used to calculate the capture velocity as $v_c = \mu + 2\sigma$, presented in Tab. 18. Velocity distribution for caesium is comparable to the one of proof-of-concept simulation.

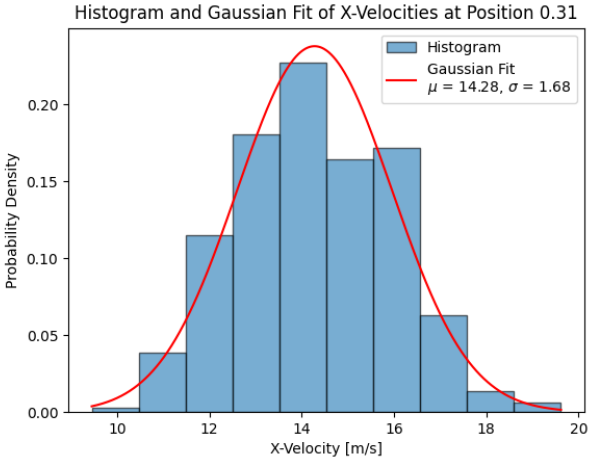

(a)

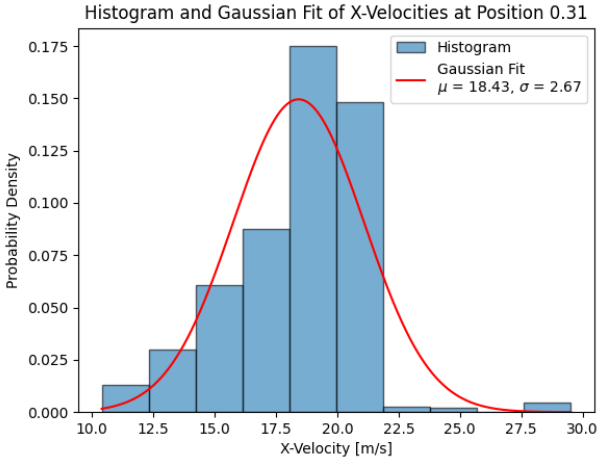

(b)

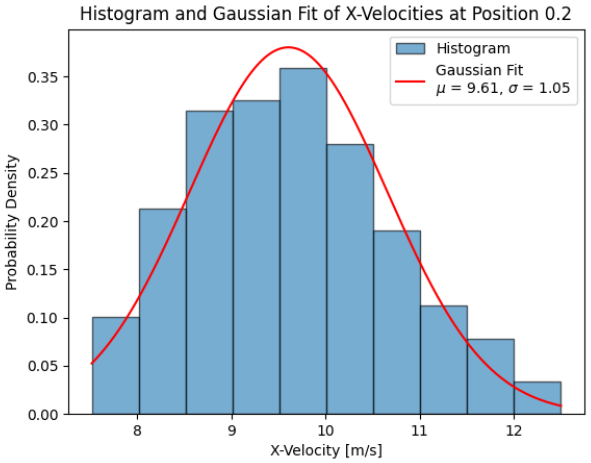

(c)

Figure 15: Velocity distribution of an atomic beam before 3D MOT, with a Gaussian fit, for a) caesium, b) potassium, and c) silver atoms.

In Fig. 14 we present three stages of the atomic movement in the system. In

Fig. 14b we present the atomic cloud attracted towards the centre through the trapping volume of the magnetic field (blue ellipsoid). Since the velocity in the X-axis is not limited they escape from both sides. Atoms pushed to the very centre encounter the push beam causing them to travel through the differential pumping tube. Atoms pushed by the beam travel between the 2D MOT and 3D MOT. The gravitational force causes a shift in the Z position which was accounted for in the design. This shift stops interaction with the push beam. In Fig. 14c we can see a 3D MOT trapping the atoms. Those stages are also resembled in the velocity change shown in Fig. 16. First, it decreases and fluctuates when trapped in 2D MOT, then the velocity increases with the acceleration of the push beam. We see a plateau when the atoms fall away from the laser light. When they enter the 3D MOT they experience a small velocity jump when it is attracted to the centre and then a sudden decrease due to the cooling. After small fluctuations due to position changes around the centre they are cooled completely.

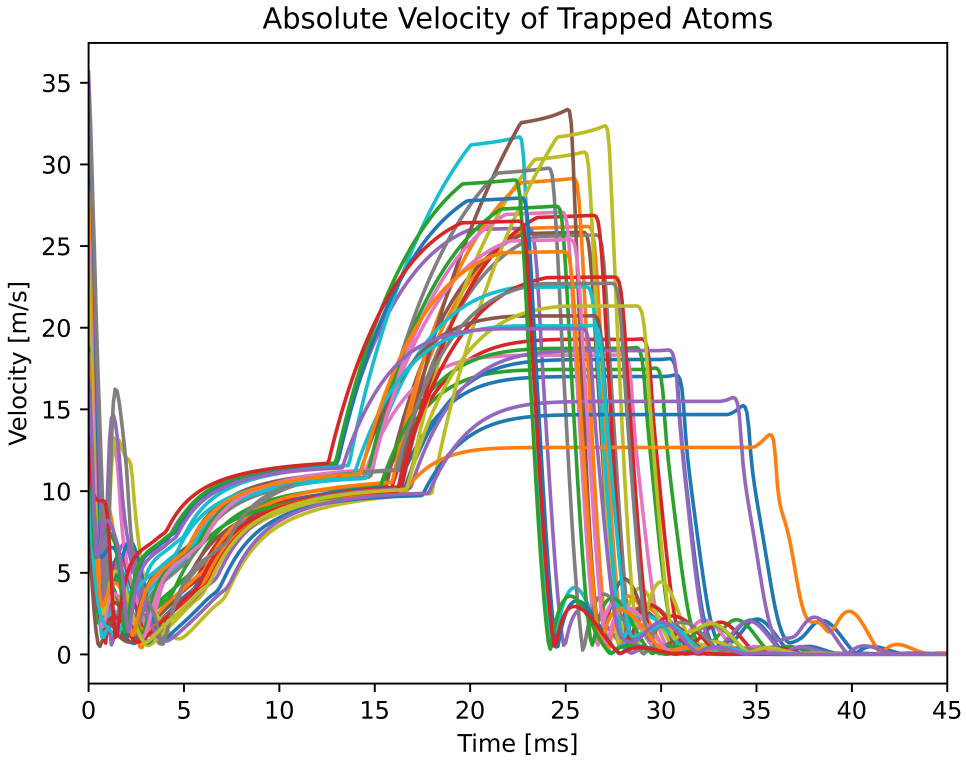

Figure 16: Absolute velocity of caesium atoms through time that has been trapped. For clarity, we have outlined 5% of all atoms.

We have calculated the trapping rate for each layout. For caesium, flux is of the order represented in the documented experiment [22] but since we don't include the desorption of the caesium atoms from the walls we can expect a one-order increase as it was the case for [22]. If we calculate the efficiency of trapping as defined in [22] we obtain 0.86% which is 100x more efficient than the previous trap. Because the trap is much smaller it results in a similar flux but much higher efficiency. It's a consequence of optimising the trap based on its efficiency not on

the outgoing flux or trapping rate. We will further explore this scheme widening the trap and performing optimisation using trapping rate as score.

Table 18: Calculated values obtained from the simulation for potassium, caesium, and silver segments.

	Cs	K	Ag
L [atoms/s]	$5.95 \cdot 10^7$	$1.87 \cdot 10^{10}$	$3.12 \cdot 10^{10}$
Φ_{2D} [atoms/s]	$6.21 \cdot 10^7$	$1.89 \cdot 10^{10}$	$7.30 \cdot 10^{10}$
v_c [m/s]	17.45	25.56	12.16
α	$7.0 \cdot 10^{-5}$	$5.6 \cdot 10^{-5}$	$1.9 \cdot 10^{-5}$

The potassium system was estimated to have the same order trapping rate as the known source [21] (since only 2D+MOT was analysed by the other group we assume 100% trapping efficiency between 2D+ and 3D MOT). We can presume that when the second laser cooling wavelength is implemented the trapping rate will grow. As for silver, we saw a great improvement compared with the setup of Gerald Uhlenberg [25]. With growing new laser technologies we have 200 times more output power than 20 years ago. This allowed us to use a 2D+ 3D MOT scheme, which as we can see, traps atoms more efficiently. We do not have a clear picture of how big collision losses will be but we can presume, with such a good estimated value, the trapping rate will be substantial nevertheless.

6.3 Possible improvements

We have used three different programming languages to realise those calculations and they were executed independently. In the future, we want to create a single Matlab app. It will provide space for inserting each parameter, it will visualise the system so that it will be easier to design it, and, when ready, it will execute Rust AtomECS software to calculate the trajectories. Then it will calculate the evaluation parameters, like flux or trapping rate, and provide velocity distribution at a selected plane. It will be easy to use and open to new users. The simulation didn't include collisions, which are computationally draining but could be implemented with a specific exponent factor depending on time spent by atom in the trap. Allowing a single simulation to have more than one transition used for laser cooling would permit simulating the influence of the repump beam and discussing bi-colour traps. We have created a script that would perform a simulation of a system with MOTs of different colours. This should be evaluated by comparing it with a well-documented experiment [64]. The final improvement would be to perform the Bayesian optimisation in terms of the final trapping rate not the trapping efficiency of the system.

7 Conclusion

In this work, we have successfully presented a program to simulate, characterise and optimize a composite magneto-optical trap setup. Our base was AtomECS software which we have modified to allow for more compound simulation. We wrote an additional Python script for the analysis of trajectories of atoms according to the established theoretical model and a Matlab script that optimised parameters and visualised atoms in the system.

In order to show that our model performs no worse than the established solutions we simulated three different documented experimental setups each that worked with an atomic species of our interest, caesium, potassium and silver. The original simulation for the experimental setup of a 2D+ 3D MOT used for trapping and cooling ^{133}Cs atoms [22] estimated the trapping rate to be $5(4) \cdot 10^7$ [atoms/s]. We estimated it as $0.618(5) \cdot 10^7$ [atoms/s] which is 1.1 standard deviation away making it not statistically different. For this setup, we also showed agreement for trapping efficiency, and capture velocity. For a 2D MOT that was a source of cold ^{39}K atoms [21], the original simulation estimated the flux to be $8.7 \cdot 10^{10}$ [atoms/s] which was an order larger than what we have calculated $2.5(5) \cdot 10^9$ [atoms/s]. We explained this discrepancy as a loss due to the simulation of only one cooling frequency out of two that were used in the original experiment.

We successfully simulated a system that is currently in construction. It is designed to create weakly bound molecules of KAg and CsAg. The design consists of two 2D magneto-optical traps and one common 3D MOT. We have performed simulations for every atomic species and calculated the trapping rate, trapping efficiency, capture velocity, and flux before the 3D MOT. We have optimised the system's parameters for the highest possible trapping efficiency. The final calculated trapping rate was $L_{\mathrm{Cs}} = 5.95 \cdot 10^7$ [atoms/s] for caesium, $L_{\mathrm{K}} = 1.87 \cdot 10^{10}$ [atoms/s] for potassium, and $L_{\mathrm{Ag}} = 3.12 \cdot 10^{10}$ [atoms/s] for silver. Each trapping rate was bigger or comparable to the values achieved in the documented experiments. Especially the segment for cooling silver atoms provided much higher trapping rate than what was observed in the documented experiment. We also proposed improvements to the code, enabling the simultaneous simulation of traps with different frequencies, and making the software more user-friendly and accessible.

Appendix A

The full script of the simulation program is available on GitHub

`https://github.com/MichalMaryn/MOT-simulation.git`.

References

[1] C. C. W. Taylor. *The Atomists: Leucippus and Democritus: Fragments*, volume 5 of *Phoenix Presocratics*. University of Toronto Press, Toronto, 1999.

[2] Robert Boyle. *The Sceptical Chymist*. J. Cadwell, London, 1661.

[3] John Dalton. *A New System of Chemical Philosophy*. Bickerstaff, London, 1808.

[4] J. J. Thomson. Cathode rays. *Philosophical Magazine*, 44(269):293–316, 1897.

[5] Ernest Rutherford. The scattering of α and β particles by matter and the structure of the atom. *Philosophical Magazine*, 21(125):669–688, 1911.

[6] Erwin Schrödinger. An undulatory theory of the mechanics of atoms and molecules. *Physical Review*, 28:1049–1070, 1926.

[7] Werner Heisenberg. Über den anschaulichen inhalt der quantentheoretischen kinematik und mechanik. *Zeitschrift für Physik*, 43:172–198, 1927.

[8] Albert Einstein. Quantentheorie des einatomigen idealen gases. *Sitzungsberichte der Preussischen Akademie der Wissenschaften, Physikalisch-Mathematische Klasse*, pages 3–14, 1925.

[9] Satyendra Nath Bose. Planck's law and the hypothesis of light quanta. *Zeitschrift für Physik*, 26(1):178–181, 1924.

[10] T. W. Hänsch and A. L. Schawlow. Cooling of gases by laser radiation. *Optics Communications*, 13(1):68–69, 1975.

[11] E. L. Raab, M. Prentiss, A. Cable, S. Chu, and D. E. Pritchard. Trapping of neutral sodium atoms with radiation pressure. *Physical Review Letters*, 59(23):2631–2634, 1987.

[12] M. H. Anderson, J. R. Ensher, M. R. Matthews, C. E. Wieman, and E. A. Cornell. Observation of bose-einstein condensation in a dilute atomic vapor. *Science*, 269(5221):198–201, 1995.

[13] Richard P. Feynman. Simulating physics with computers. *International Journal of Theoretical Physics*, 21:467–488, 1982.

[14] Seth Lloyd. Universal quantum simulators. *Science*, 273(5278):1073–1078, 1996.

[15] Iulia Georgescu, S. Ashhab, and Franco Nori. Quantum simulation. *Reviews of Modern Physics*, 86, 08 2013.

[16] M Ortner, A Micheli, G Pupillo, and P Zoller. Quantum simulations of extended hubbard models with dipolar crystals. *New Journal of Physics*, 11(5):055045, May 2009.

[17] Herman Feshbach. Unified theory of nuclear reactions. *Annals of Physics*, 5(4):357–390, 1958.

[18] Michał Śmiałkowski and Michał Tomza. Highly polar molecules consisting of a copper or silver atom interacting with an alkali-metal or alkaline-earth-metal atom. *Physical Review A*, 103(2), February 2021.

[19] M. Aymar and O. Dulieu. Calculation of accurate permanent dipole moments of the lowest Σ+1,3 states of heteronuclear alkali dimers using extended basis sets. *The Journal of Chemical Physics*, 122(20):204302, 05 2005.

[20] Marin Pichler, David Hall, Michael Garman, and Daniel Barker. Dual potassium-cesium mot for production of ultracold molecules. In *41st Annual Meeting of the APS Division of Atomic, Molecular and Optical Physics*, volume 55, Houston, Texas, May 25–29 2010. American Physical Society. Abstract ID: BAPS.2010.DAMOP.E1.128.

[21] J. Catani, P. Maioli, L. De Sarlo, F. Minardi, and M. Inguscio. Intense slow beams of bosonic potassium isotopes. *Phys. Rev. A*, 73:033415, Mar 2006.

[22] Aden Zhenhao Lam, Claire Warner, Niccolò Bigagli, Stephan Roschinski, Weijun Yuan, Ian Stevenson, and Sebastian Will. Compact two-dimensional magneto-optical trap for ultracold atom setups, 2021.

[23] S. Sutradhar, A. Misra, G. Pal, S. Majumder, S. Roy, and S. Chaudhuri. Fast loaded dual-species magneto-optical trap of cold sodium and potassium atoms with light-assisted inter-species interaction. *AIP Advances*, 2023. Dated: 23 August 2023. Electronic mail: srishic@rri.res.in.

[24] J. Q. Huang, X. S. Yan, C. F. Wu, J. W. Zhang, Y. Y. Feng, and L. J. Wang. Intense source of cold cesium atoms based on a two-dimensional magneto-optical trap with independent axial cooling and pushing, 2015.

[25] G. Uhlenberg, J. Dirscherl, and H. Walther. Magneto-optical trapping of silver atoms. *Phys. Rev. A*, 62:063404, Nov 2000.

[26] S. Yang, M. Verma, R. Kapur, J. Dewhurst, T.K. Langin, W. Cassidy, A. O. Jamison, and D. DeMille. Magneto-optical trapping of silver atoms towards ultracold ^{223}FrAg molecules to probe nuclear cp-violation. In *55th Annual Meeting of the APS Division of Atomic, Molecular and Optical Physics*, Fort Worth, Texas, June 2024. American Physical Society.

[27] Mariusz Semczuk. Private communication, 2024.

[28] T. G. Tiecke, S. D. Gensemer, A. Ludewig, and J. T. M. Walraven. High-flux two-dimensional magneto-optical-trap source for cold lithium atoms. *Physical Review A*, 80(1), July 2009.

[29] Ingo Nosske, Luc Couturier, Fachao Hu, Canzhu Tan, Chang Qiao, Jan Blume, Y. H. Jiang, Peng Chen, and Matthias Weidemüller. Erratum: Two-dimensional magneto-optical trap as a source for cold strontium atoms [phys. rev. a 96 , 053415 (2017)]. *Physical Review A*, 97(3), March 2018.

[30] Shuwei Jin, Jianshun Gao, Karthik Chandrashekara, Christian Gölzhäuser, Joschka Schöner, and Lauriane Chomaz. Two-dimensional magneto-optical trap of dysprosium atoms as a compact source for efficient loading of a narrow-line three-dimensional magneto-optical trap. *Physical Review A*, 108(2), August 2023.

[31] H. J. Metcalf and P. van der Straten. *Atoms and Molecules Interacting with Light: Atomic Physics for the Laser Era*. Cambridge University Press, Cambridge, 1999.

[32] J. J. Sakurai. *Modern Quantum Mechanics*. Addison-Wesley Publishing Company, Inc., revised edition edition, 1994. Pages 14, 16.

[33] Sven Abend, Baptiste Allard, Aidan Arnold, Ticijana Ban, Liam Barry, Baptiste Battelier, Ahmad Bawamia, Q. Beaufils, Simon Bernon, Andrea Bertoldi, Alexis Bonnin, Philippe Bouyer, Alexandre Bresson, Oliver Burrow, Benjamin Canuel, Bruno Desruelle, Giannis Drougakis, René Forsberg, Naceur Gaaloul, and Michał Zawada. Technology roadmap for cold-atoms based quantum inertial sensor in space. *AVS Quantum Science*, 5:019201, 03 2023.

[34] D. Budker, D. F. Kimball, and D. P. DeMille. *Atomic Physics*. Oxford University Press, Padstow, Cornwall, UK, 2004.

[35] Jakub Spiechowicz, Ivan G. Marchenko, Peter Hänggi, and Jerzy Łuczka. Diffusion coefficient of a brownian particle in equilibrium and nonequilibrium: Einstein model and beyond. *Entropy*, 25(1):42, 2023.

[36] Daniel A. Steck. Cesium d line data, 2010. Version 2.3.3, revised May 28, 2024.

[37] Donald M. Mattox. Chapter 6 – vacuum evaporation and vacuum deposition. In *Handbook of Physical Vapor Deposition*, 2010.

[38] Walter Kauzmann. *Kinetic Theory of Gases*. W. A. Benjamin, New York, dover ed., republished in 2012 edition, 1966.

[39] V. P. Itkin C. B. Alcock and M. K. Horrigan. Vapour pressure equations for the metallic elements: 298–2500k. *Canadian Metallurgical Quarterly*, 23(3):309–313, 1984.

[40] John E. Mahan. *Physical Vapor Deposition of Thin Films*. John Wiley & Sons, New York, 2000.

[41] J. González-Leal. Optical functionalities of dielectric material deposits obtained from a lambertian evaporation source. *Optics express*, 15:5451–9, 05 2007.

[42] P. Clausing. Über die strahlformung bei der molekularströmung. *Zeitschrift für Physik*, 66(7):471–476, 1930.

[43] R.M Lowe. The evaporation of silver in oxygen, nitrogen and vacuum. *Acta Metallurgica*, 12(10):1111–1118, 1964.

[44] F. London. The general theory of molecular forces. *Transactions of the Faraday Society*, 33:8B, 1937. Published on 01 January 1937.

[45] H. Margenau, N. R. Kestner, and D. ter Haar. *Theory of Intermolecular Forces*. Pergamon Press, 1969.

[46] J. Terpstra and J. A. Smit. Measurement of "optical" transition probabilities in the silver atom. *Physica*, 24(6-10):937–958, 1958.

[47] A. M. Steane, M. Chowdhury, and C. J. Foot. Radiation force in the magneto-optical trap. *J. Opt. Soc. Am. B*, 9(12):2142–2158, Dec 1992.

[48] Hong-Shan Zhang, Zhong-Hua Ji, Jin-Peng Yuan, Yan-Ting Zhao, Jie Ma, Li-Rong Wang, Lian-Tuan Xiao, and Suo-Tang Jia. Cold cesium molecules produced directly in a magneto—optical trap. *Chinese Physics B*, 20(12):123702, 2011.

[49] H. Wang, P. L. Gould, and W. C. Stwalley. Photoassociative spectroscopy of ultracold ^{39}K atoms in a high-density vapor-cell magneto-optical trap. *Phys. Rev. A*, 53:R1216–R1219, Mar 1996.

[50] D. Wang, J. Qi, M. F. Stone, O. Nikolayeva, B. Hattaway, S. D. Gensemer, H. Wang, W. T. Zemke, P. L. Gould, E. E. Eyler, and W. C. Stwalley. The photoassociative spectroscopy, photoassociative molecule formation, and trapping of ultracold ^{39}K^{85}Rb. *The European Physical Journal D*, 31(2):165–177, November 2004.

[51] T. G. Tiecke. Properties of potassium, 2019.

[52] Z. Zhang, N. X. Nie, R. A. Mendybaev, M.-C. Liu, K. D. McKeegan, and N. Dauphas. Evaporation kinetics of potassium and rubidium and their isotope fractionation under vacuum conditions. In *51st Lunar and Planetary Science Conference*, page Abstract #2341, 2020.

[53] D. R. Smith and F. R. Fickett. Low-temperature properties of silver. *Journal of Research of the National Institute of Standards and Technology*, 100(2):119–171, March-April 1995.

[54] P. L. Larkins and P. Hannaford. Precision measurement of the energy of the $4d^9\ 5s_2D_{5/2}$ metastable level in Ag I. *Zeitschrift für Physik D Atoms, Molecules and Clusters*, 32(3):167–172, 1994.

[55] S. Eckel, D. S. Barker, E. B. Norrgard, and J. Scherschligt. Pylcp: A python package for computing laser cooling physics, 2020.

[56] X. Chen, M. Zeuner, U. Schneider, C. J. Foot, T. L. Harte, and E. Bentine. Atomecs: Simulate laser cooling and magneto-optical traps, 2021.

[57] X. Chen, M. Zeuner, U. Schneider, C. J. Foot, T. L. Harte, and E. Bentine. Atomecs github repository. `https://github.com/TeamAtomECS/AtomECS/blob/master/examples/1d_mot.rs`, 2022.

[58] David J. DeTroye and Ronald J. Chase. The calculation and measurement of helmholtz coil fields. Technical Report ADA286081, Army Research Laboratory, Adelphi, MD, 1994. Final report, October 1993–October 1994.

[59] Aden Zhen Hao Lam. *Ultracold dipolar gases of NaCs ground state molecules*. Phd thesis, Columbia University, Columbia, USA, 2022.

[60] Jacopo Catani. *A New Apparatus for Ultracold K-Rb Bose-Bose Atomic Mixtures*. Phd thesis, Università degli Studi di Firenze, Dipartimento di Fisica, Firenze, Italy, December 2006. Dottorato di Ricerca in Fisica, XIX Ciclo.

[61] Gerald Uhlenberg. *Einfang von Silberatomen in einer magneto-optischen Strahlungsdruckfalle*. Phd thesis, Ludwig-Maximilians University, Munich, Germany, Feb 2000.

[62] Paweł Arciszewski. *An experimental apparatus for laser cooling of potassium and caesium*. PhD thesis, University of Warsaw, 2019.

[63] Mateusz Bocheński, Jakub Dobosz, and Mariusz Semczuk. Magnetic trapping of an ultracold ^{39}K-^{40}K mixture with a versatile potassium laser system, 2024.

[64] Jianshun Gao. A first two-dimensional magneto-optical trap for dysprosium. Master's thesis, University of Heidelberg, Heidelberg, Germany, 2022.